PFC/RR-88-9

TSC Simulations of Alcator C-MOD Discharges I: A Vertically Symmetric Scenario

Ramos, J. J.

Plasma Fusion Center
Massachusetts Institute of Technology
Cambridge, MA 02139

July, 1988

This work was supported by the U. S. Department of Energy Contract No. DE-AC02-78ET51013. Reproduction, translation, publication, use and disposal, in whole or in part by or for the United States government is permitted.

TSC Simulations of Alcator C-Mod Discharges

I: A Vertically Symmetric Scenario

J. J. Ramos

MIT Plasma Fusion Center

ABSTRACT

The Tokamak Simulation Code (TSC) is used to model the evolution of a full performance three second discharge of the Alcator C-MOD tokamak. Perfect symmetry about the equatorial plane is assumed in this simulation.

The Tokamak Simulation Code (TSC)[1] is an axisymmetric, time dependent code that models the evolution and control properties of a tokamak on the transport time scale. It encompasses a full non-linear set of two fluid plasma transport equations in two non-ignorable spatial dimensions. The plasma interacts with a set of axisymmetric conductors that model the passive metalic structure around it, as well as the active poloidal field (PF) coils. These conductors obey electromagnetic circuit equations with active feedback systems included. Such a code is a most valuable tool to investigate the positional stability and control issues associated with the operation of shaped tokamaks. We have embarked in a program of extensive TSC code use in order to simulate Alcator C-Mod discharges. The present report summarizes the first phase of these studies in which, for simplicity, we have made the assumption of perfect (up-down) symmetry about the equatorial plane. This precludes the investigation of vertical stability and control issues which will be dealt with in the next phase of our studies. Nevertheless, within the assumption of vertical

symmetry we can address a number of important issues such as plasma current ramp-up and ramp-down control, radial position control, flux consumption and pulse length, separatrix formation and diverted operation, and PF coil requirements.

Our computational grid covers a 0.88 m wide by 1.48 m high rectangle in the meridian plane, with mesh points 0.02 m apart as shown in Fig.1. The vacuum vessel is represented by a set of discrete coils whose location is also displayed in Fig.1. The PF coils located inside the computational domain are also represented by sets of filaments, one on every grid point within the actual dimensions of the coil. The following table compares the number of filaments used to model each coil with the actual number of turns in the coil design (upper or lower half only).

TABLE 1

COIL	NO. OF FILAMENTS IN OUR MODEL	ACTUAL NUMBER OF TURNS
OH1 (nose)	20	34
OH1 (ear)	18	31
OH2	18	27
EF1	25	94
EF2	25	97
EF3	28	75
VACUUM VESSEL	65	

The only coil located outside the computational grid is EF4, which is modeled as a single filament at its geometrical center.

We set out to simulate a full performance discharge of 3s duration. The current rise phase takes 1s and is followed by a 1s flat-top at 3 Mamp of plasma current, and a ramp-

down phase that brings the plasma current back to zero in another second. The vacuum toroidal field is varied in time. At the moment of plasma initiation we have a toroidal magnetic field of 6T at R = 0.665 m. This field is increased linearly in time to reach 9T at the beginning of the flat-top phase. It stays constant at 9T through the flat-top and is brought down to 6T during the current ramp-down. Figures 2 and 3 show the time dependence of the plasma current and the toroidal field.

Our simulation starts shortly after the plasma breakdown. At this point we initiate the TSC run with a low current (50 Kamp), low pressure ($\beta = 10^{-5}$) plasma equilibrium. This initial plasma is roughly circular and leans against the inboard limiter at R = 0.430 m. It is held by an external poloidal field that departs only slightly from a perfect null at a poloidal flux of -2.88 Volt-s. Figure 5 displays the toroidal current density and the poloidal flux for this initial equilibrium.

As time proceeds, the plasma current is inductively increased by the appropriate variation of the PF flux, so as to follow the time history indicated in Fig.2. Plasma fueling is simulated by a prescribed time dependence of the particle density which is shown in Fig.4. The plasma temperature increases as the result of ohmic heating. No auxiliary heating is included in the present simulation. The plasma volume is increased by increasing both the minor radius and the elongation. One of the objectives of our simulation is to achieve a full-sized, diverted plasma as early as possible in the discharge. This is reached at t = 0.24 s when the plasma current equals 1.5 Mamps. Thereafter the geometry of the plasma boundary and the location of the x-point remain virtually constant for the remainder of the ramp-up phase and till the end of the flat-top. Figures 6 and 7 illustrate the equilibrium configurations at t = 0.34 s, i.e. a little after the diverted state has been reached, and at t = 2.00 s, i.e. at the end of the flat-top. The time dependence of the major radius, minor radius, elongation, triangularity and x-point coordinates is shown in Figs. 8 through 13. In its quiescent phase, the plasma major radius equals 0.655 m, the minor radius is equal to 0.223 m and the coordinates of the x-point are $R_x = 0.56$ m and $Z_x = 0.41$ m. Thus the x-point-defined elongation and triangularity are $\kappa_x = 1.86$ and $\delta_x = 0.48$. At the 95% relative to the separatrix flux surface the elongation and triangularity are $\kappa_{95} = 1.62$ and $\delta_{95} = 0.31$. During the ramp-down phase the plasma current is decreased linearly down to 63 Kamp. at t = 3.00 s. In this phase the plasma shrinks in size but remains elongated and diverted throughout. Figure 14 summarizes the evolution of the plasma shape through the current ramp-up and flat-top, whereas Fig.15 does so for the ramp-down phase.

The evolution of the plasma current and geometrical parameters is controlled by the appropriate values of the PF coil currents as functions of time. These are arrived at as the result of a judicious preprogramming of the coil current time histories superposed on which are a number of active feedback systems. The first one acts on coil EF3 and controls the radial position of the plasma (i.e. keeps it centered about 0.665 m for the quiescent phase). The second one acts on a linear combination of OH2, EF1 and EF2 that produces an approximate quadrupole field, and controls the plasma elongation. Finally a combination of OH1, OH2, EF1, EF2 and EF3 that produces an approximate field null is used to control the evolution of the plasma current.

The safety factor q and the ratio of kinetic to magnetic pressure β are crucial parameters in ideal MHD stability considerations. They are displayed as functions of time in Figs. 16 and 17. We note that the low β inherent to the high field Alcator design will keep the plasma stable against pressure driven modes. The value of the safety factor, $q \simeq 2.5$ at the 95% flux surface should be sufficient to prevent current driven kink instabilities.

The peak electron temperature and the confinement time are shown in Figs. 18 and 19. Our simulation predicts nearly 4 KeV of maximum temperature and a confinement time somewhat above 60 ms. However, a word of caution should be said about these estimates. The TSC code has an artificial way of modeling the sawtooth behavior that preserves the axisymmetry. Namely wherever q falls below unity, the plasma resistivity is enhanced until the current density is sufficiently low to keep q equal to or above one. In a relatively high current discharge like the one under consideration, this results in a large portion of the plasma where q is equal to one and the resistivity is artificially high. Consequently the central temperatures may be overestimated and the confinement time may be underestimated. This should also result in a pessimistic estimate of the flux consumption.

The poloidal flux consumption is illustrated in Fig.20. We start our simulation (right after plasma breakdown) at -2.88 volt-s. The flux swings to a maximum of +3.61 volt-s at the end of the flat-top. Thus we consume a total of 6.5 volt-s which should be within the capabilities of the machine. In calculating the plasma resistivity, Z_{eff} was set equal to 1.5 throughout the discharge.

The time histories of the PF coil currents are shown in Figs. 21 through 26 along with the corresponding voltages. Quantities plotted correspond to one filament of our model, so that use of Table 1 should be made to calculate the corresponding values per actual turn or for the whole coil. Figure 27 shows the induced currents in the vacuum vessel. All coil currents are within the engineer specified allowances. In addition, we have satisfied a number of further constraints aimed at optimizing the use of power suplies. These are as follows: The current in coils OH1, OH2 and EF2 starts with positive sign and becomes negative during the discharge, but is not allowed to go through zero again and must remain negative for the whole ramp-down phase. EF1 must have positive current through the discharge. EF3 starts with zero current which must stay below zero for the rest of the discharge. Finally EF4 is not allowed to be part of any feedback system since the thick metal between it and the plasma should result in a slow field penetration. Its current is preprogrammed to start at zero, decrease linearly to -800 Kamp at the beginning of the flat-top, stay constant through the flat-top phase, and revert to zero in the ramp-down phase.

All of these constraints can be readily met except that pertaining to EF1. We find that in order to keep the EF1 current from changing sign during the ramp-down phase, we must allow the plasma to retain its elongation through this phase. Figures 28 and 29 show the plasma elongation and EF1 current in a different ramp-down scenario in which the plasma is brought back to circular and killed against the inboard limiter as it was born. In this case the EF1 current becomes negative during the ramp-down. Since the

EF1 currents are expected to be significantly modified in an up-down asymmetric, single null discharge we think that a decision on whether the flexibility to allow negative EF1 currents is needed, should be deferred until the up-down asymmetric studies are carried out.

Acknowledgements

The author is very grateful to S. C. Jardin for providing the TSC code and offering continuous assistance in its running. This work was supported by the U.S. D.O.E.

Reference

[1] S. C. Jardin, N. Pomphrey and J. De Lucia, *J. Computational Physics* **66**, 481 (1986).

Figure Captions

Fig.1 Computational grid and model of vacuum vessel and PF coils.

Fig.2 Plasma current versus time.

Fig.3 Toroidal field stream function $(RB_t)_{\text{vacuum}}$ versus time.

Fig.4 Particle density versus time. The three traces show the central, line average and volume average values.

Fig.5 Toroidal current density and poloidal flux at initiation, t = 0.

Fig.6 Toroidal current density and poloidal flux at t = 0.34s.

Fig.7 Toroidal current density and poloidal flux at the end of flat-top, t = 2.00 s.

Fig.8 Major radius versus time.

Fig.9 Minor radius versus time.

Fig.10 Plasma elongation versus time. The different traces correspond to the 90%, 95% and edge flux surfaces. The latter is defined by either the limiter or the 99% relative to the separatrix flux surface.

Fig.11 Plasma triangularity in terms of the 90%, 95% and edge flux surfaces, versus time.

Fig.12 Radial position of the separatrix x-point versus time.

Fig.13 Axial position of the separatrix x-point versus time.

Fig.14 Evolution of the plasma edge through the current rise and flat-top.

Fig.15 Evolution of the plasma edge through the current ramp down.

Fig.16 Safety factor q versus time. The different traces correspond to the edge, the 95% flux surface, the cylindrical q and the elongation corrected cylindrical q_*.

Fig.17 Plasma beta versus time. The different traces show half the central value and the average values in terms of the volume averaged field and the vacuum field at the center respectively.

Fig.18 Peak electron temperature versus time.

Fig.19 Energy confinement time versus time.

Fig.20 Poloidal flux versus time.

Fig.21 Current and voltage in OH1 coil versus time. Magnitudes plotted correspond to one filament of our model.

Fig.22 Current and voltage in OH2 coil.

Fig.23 Current and voltage in EF1 coil.

Fig.24 Current and voltage in EF2 coil.

Fig.25 Current and voltage in EF3 coil.

Fig.26 Current in EF4 coil.

Fig.27 Induced currents in vacuum vessel versus time.

Fig.28 Plasma elongation versus time in alternate ramp-down scenario that brings the plasma shape back to circular.

Fig.29 EF1 current versus time in the alternate ramp-down scenario.

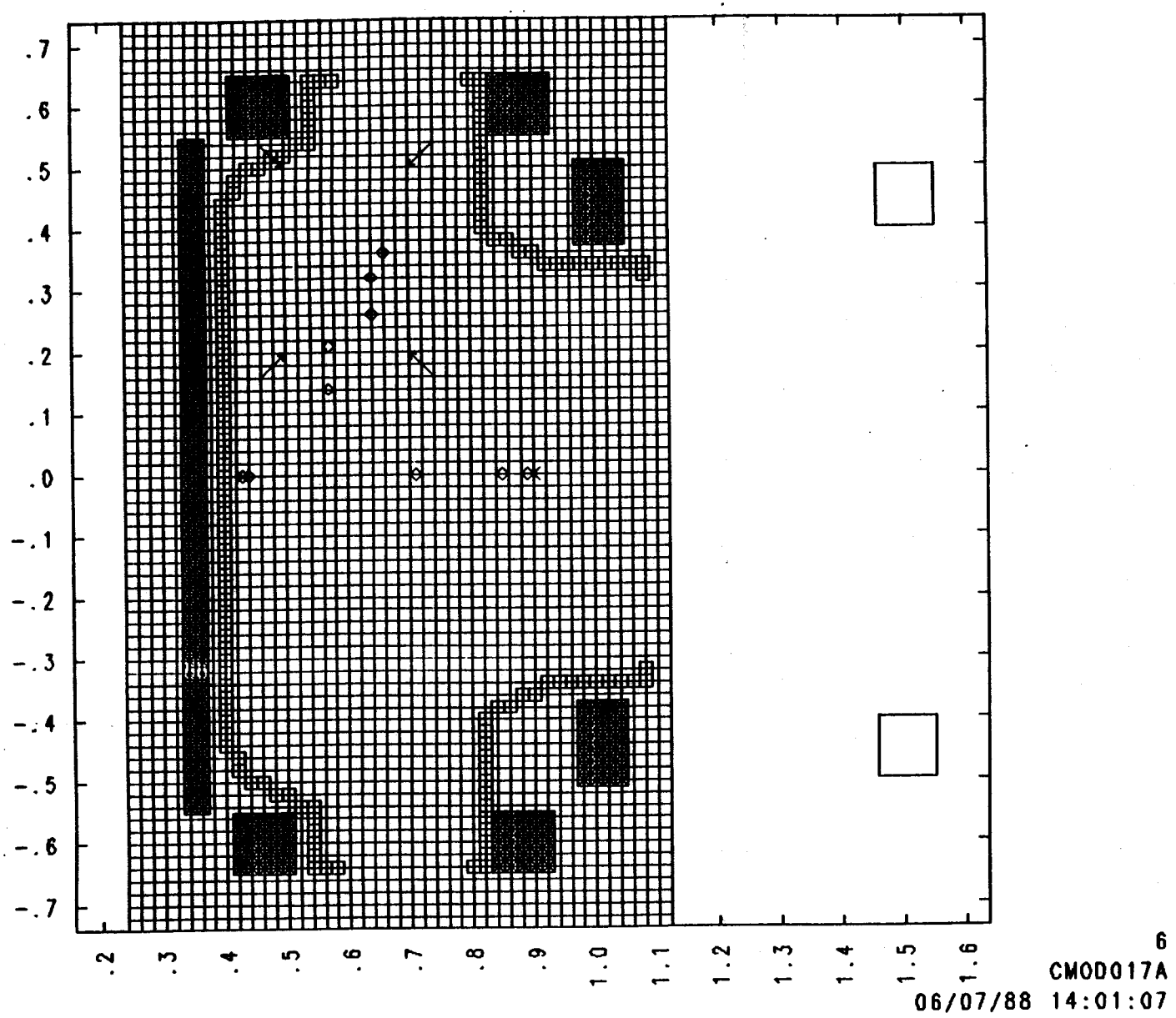
.7
.6
.5
.4
.3
.2
.1
.0
-.1
-.2
-.3
-.4
-.5
-.6
-.7
.2
.3
.4
.5
.6
.7
.8
.9
1.0
1.1
1.2
1.3
1.4
1.5
1.6
6
CMOD017A
06/07/88 14:01:07

Fig. 1

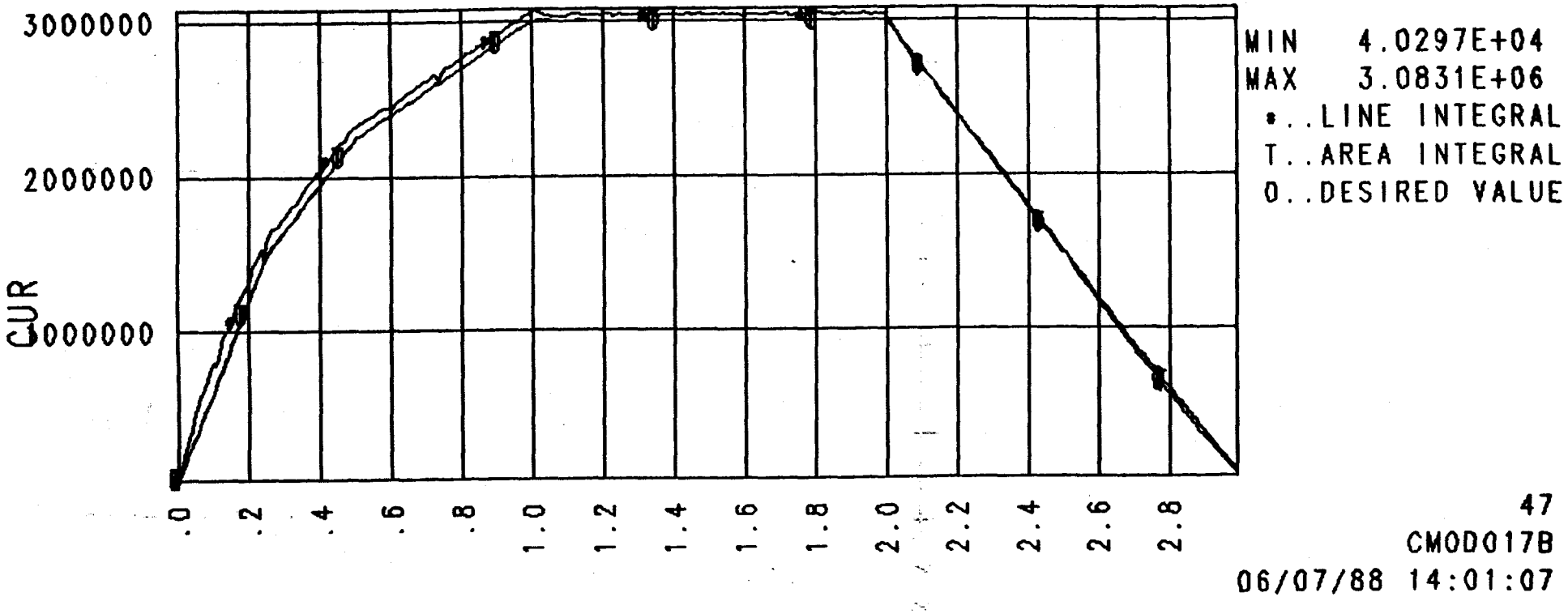
3000000
2000000
CUR
000000
.0
.2
.4
.6
.8
1.0
1.2
1.4
1.6
1.8
2.0
2.2
2.4
2.6
2.8
MIN 4.0297E+04
MAX 3.0831E+06
*..LINE INTEGRAL
T..AREA INTEGRAL
0..DESIRED VALUE
47
CMOD017B
06/07/88 14:01:07

Fig. 2

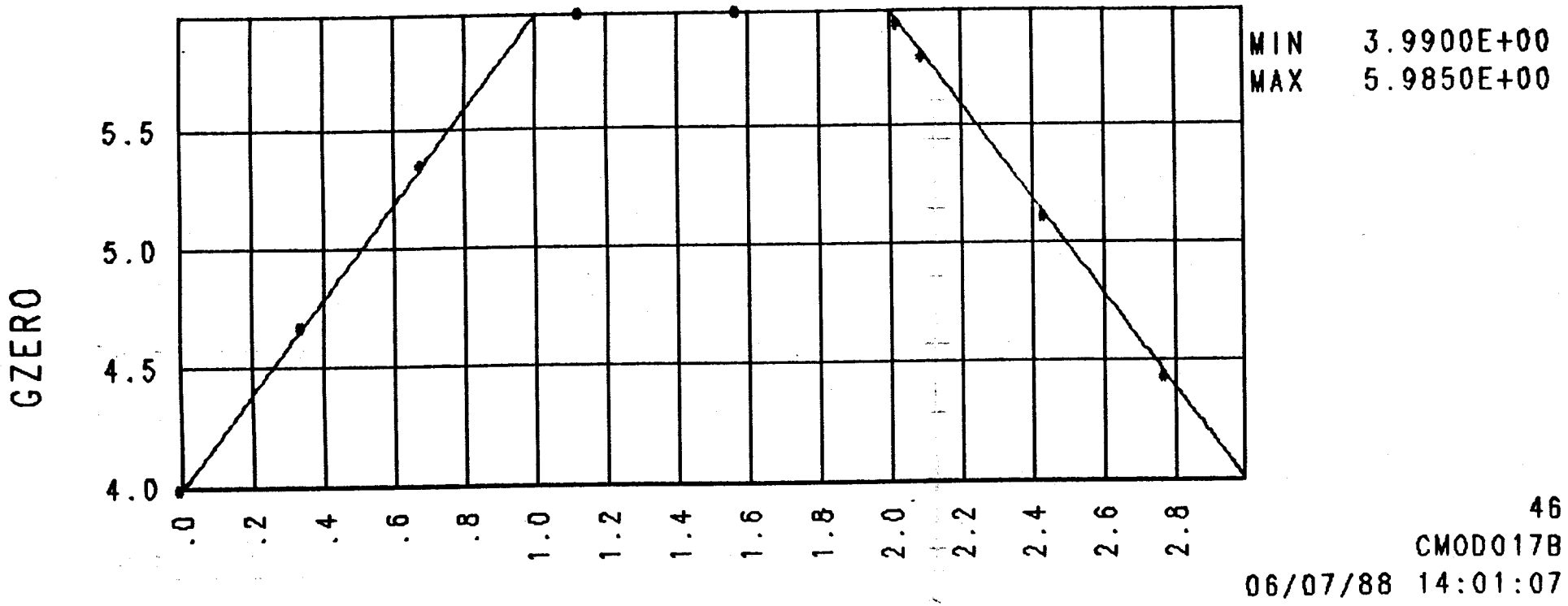
GZERO
5.5
5.0
4.5
4.0
.0
.2
.4
.6
.8
1.0
1.2
1.4
1.6
1.8
2.0
2.2
2.4
2.6
2.8
MIN 3.9900E+00
MAX 5.9850E+00
46
CMOD017B
06/07/88 14:01:07

Fig. 3

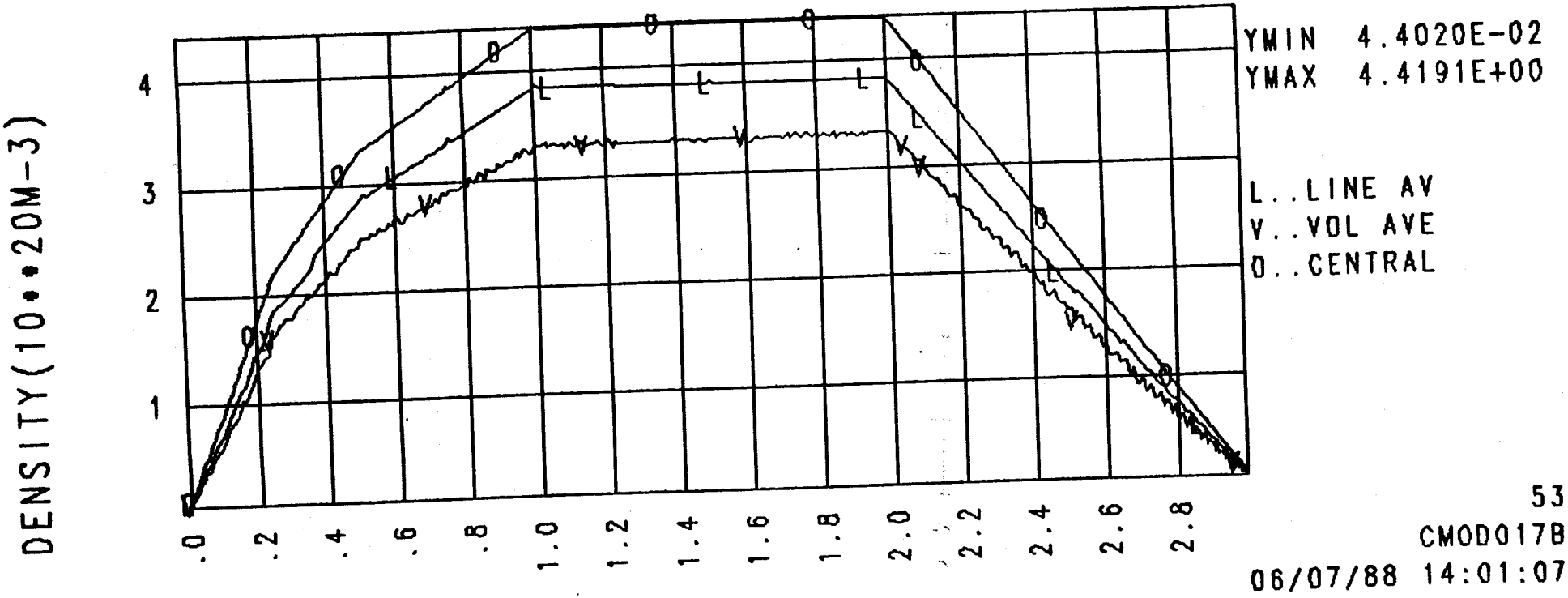
DENSITY(10**20M-3)
4
3
2
1
.0
.2
.4
.6
.8
1.0
1.2
1.4
1.6
1.8
2.0
2.2
2.4
2.6
2.8
YMIN 4.4020E-02
YMAX 4.4191E+00
L..LINE AV
V..VOL AVE
O..CENTRAL
53
CMOD017B
06/07/88 14:01:07

Fig. 4

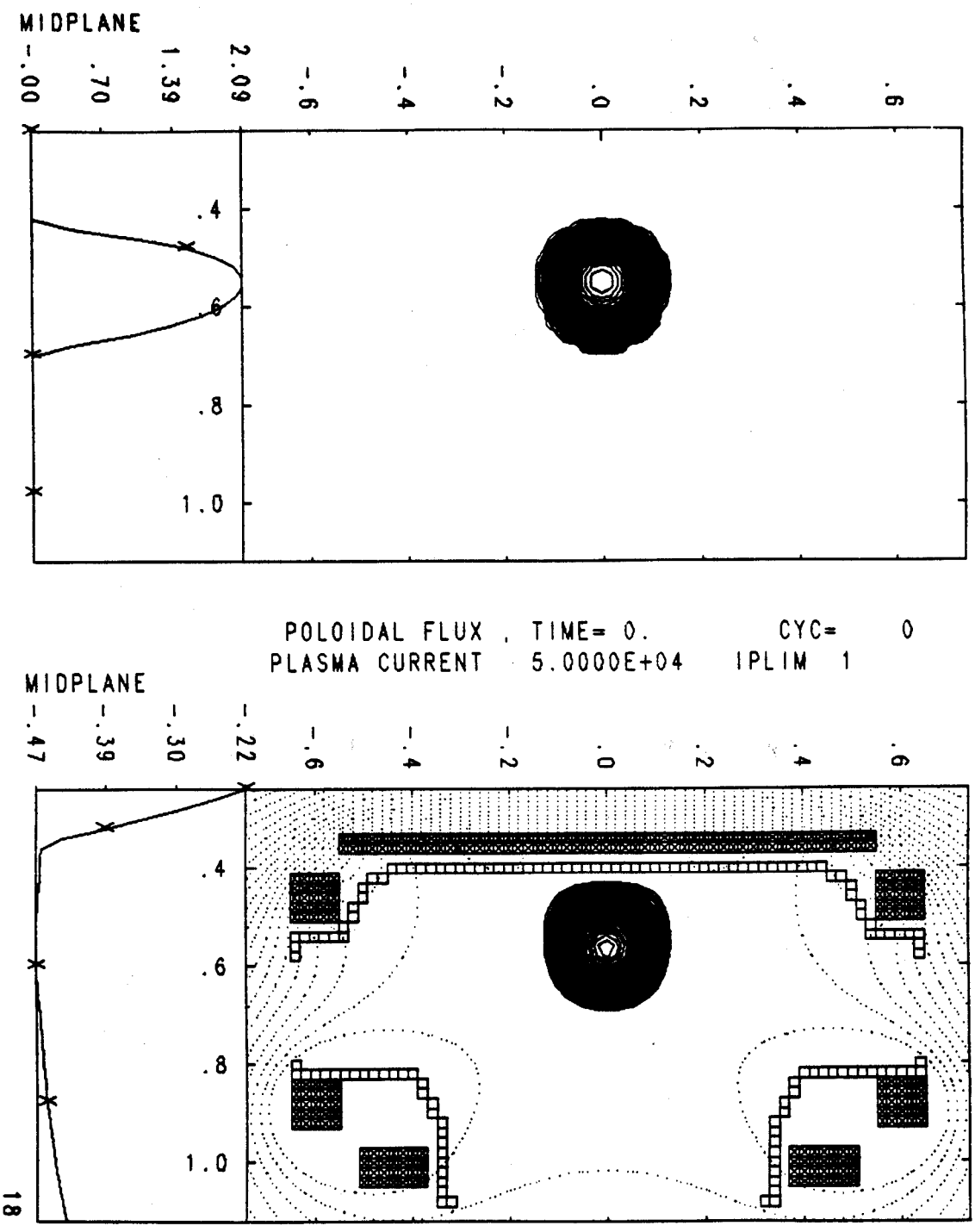
TOR CURRENT , TIME= 0. CYC= 0
MIDPLANE
-.00
.70
1.39
2.09
-.6
-.4
-.2
.0
.2
.4
.6
.4
.6
.8
1.0
POLOIDAL FLUX , TIME= 0. CYC= 0
PLASMA CURRENT 5.0000E+04 IPLIM 1
MIDPLANE
-.47
-.39
-.30
-.22
-.6
-.4
-.2
.0
.2
.4
.6
.4
.6
.8
1.0
18
CMOOO17A

Fig. 5

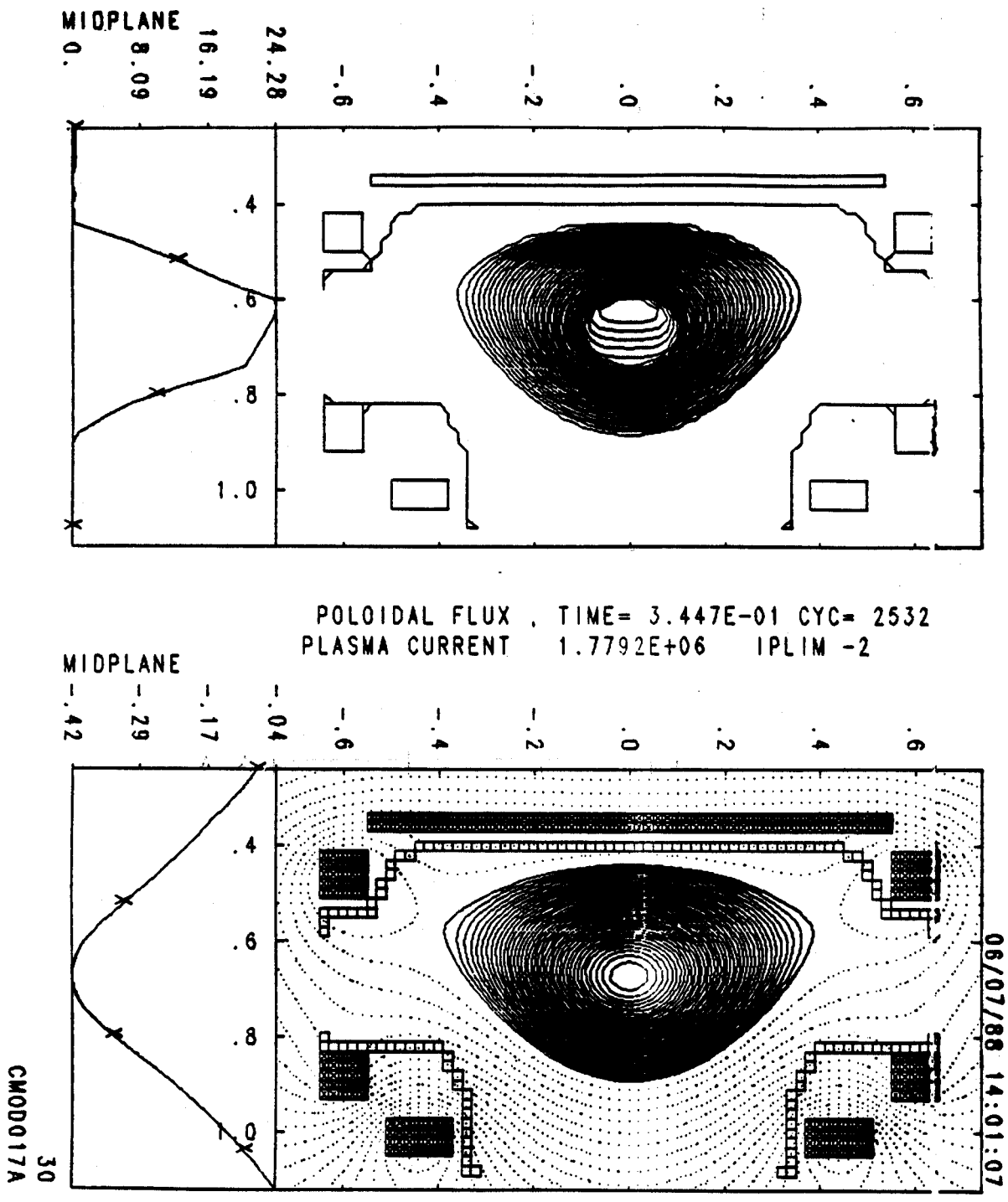
TOR CURRENT , TIME= 3.447E-01 CYC= 2532
MIDPLANE
0.
8.09
16.19
24.28
-.6
-.4
-.2
.0
.2
.4
.6
.4
.6
.8
1.0
POLOIDAL FLUX , TIME= 3.447E-01 CYC= 2532
PLASMA CURRENT 1.7792E+06 IPLIM -2
MIDPLANE
-.42
-.29
-.17
-.04
-.6
-.4
-.2
.0
.2
.4
.6
.4
.6
.8
1.0
06/07/88 14:01:07
CMOD017A
30

Fig. 6

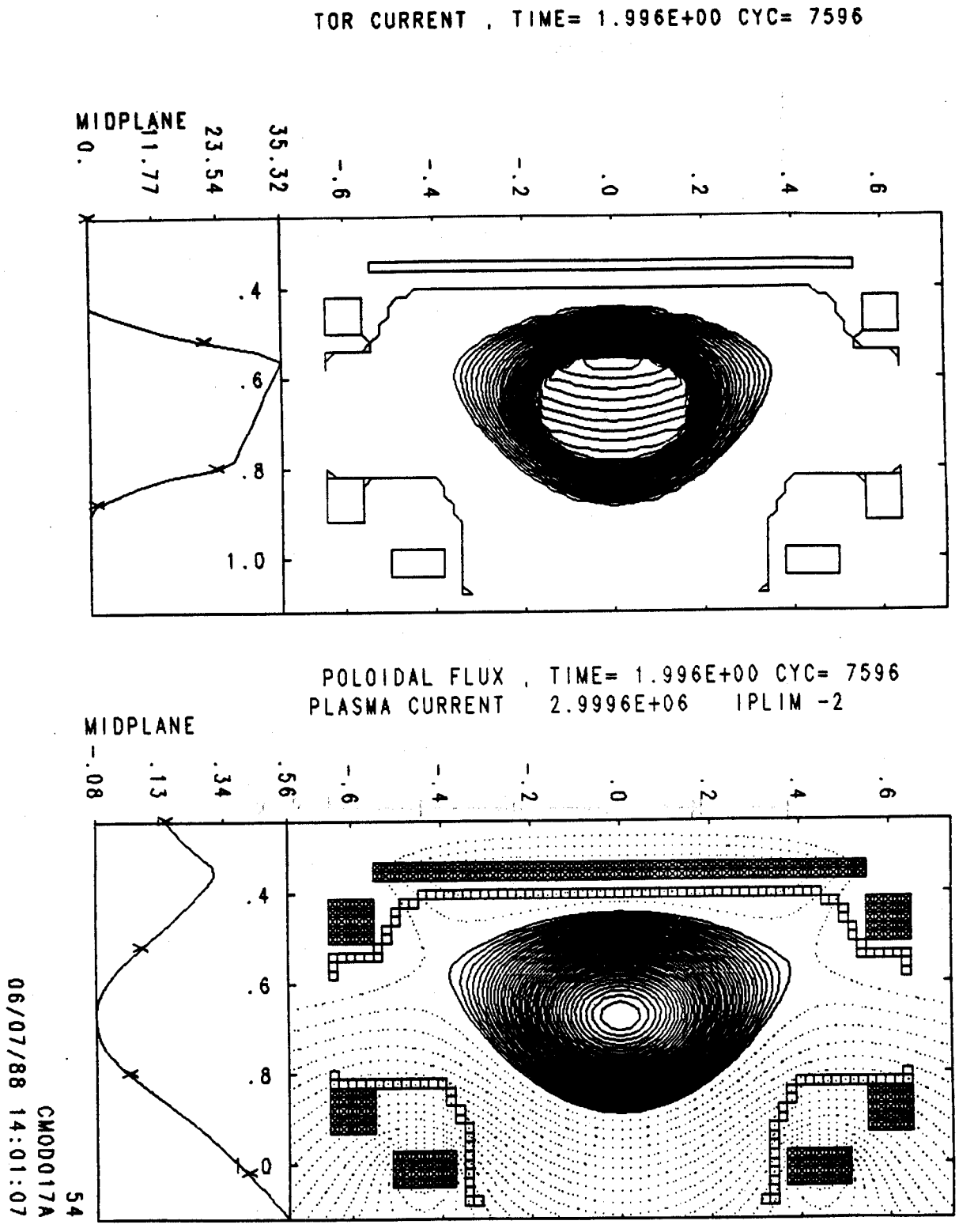
TOR CURRENT , TIME= 1.996E+00 CYC= 7596
MIDPLANE
0.
11.77
23.54
35.32
-.6
-.4
-.2
.0
.2
.4
.6
.4
.6
.8
1.0
POLOIDAL FLUX , TIME= 1.996E+00 CYC= 7596
PLASMA CURRENT 2.9996E+06 IPLIM -2
MIDPLANE
-.08
.13
.34
.56
-.6
-.4
-.2
.0
.2
.4
.6
.4
.6
.8
1.0
54
CMOD017A
06/07/88 14:01:07

Fig. 7

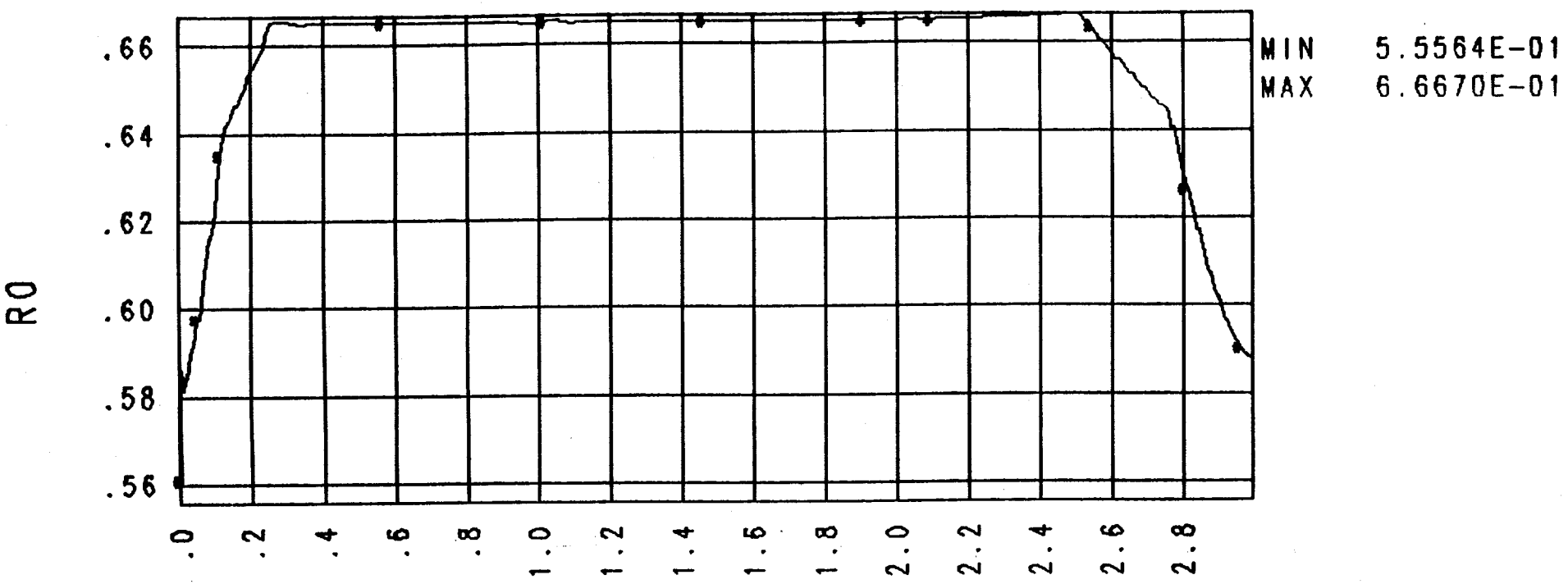
RO
.66
.64
.62
.60
.58
.56
.0
.2
.4
.6
.8
1.0
1.2
1.4
1.6
1.8
2.0
2.2
2.4
2.6
2.8
MIN 5.5564E-01
MAX 6.6670E-01

Fig. 8

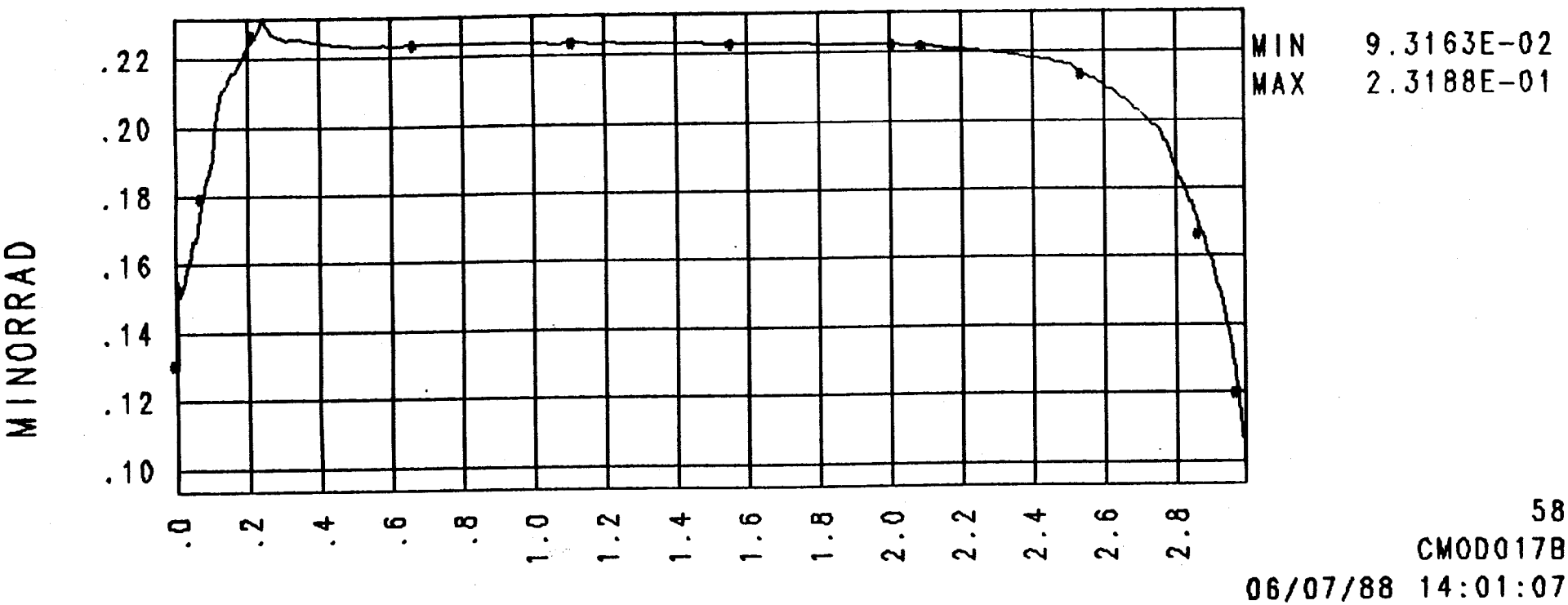
MINORRAD
.22
.20
.18
.16
.14
.12
.10
.0
.2
.4
.6
.8
1.0
1.2
1.4
1.6
1.8
2.0
2.2
2.4
2.6
2.8
MIN 9.3163E-02
MAX 2.3188E-01
58
CMOD017B
06/07/88 14:01:07

Fig. 9

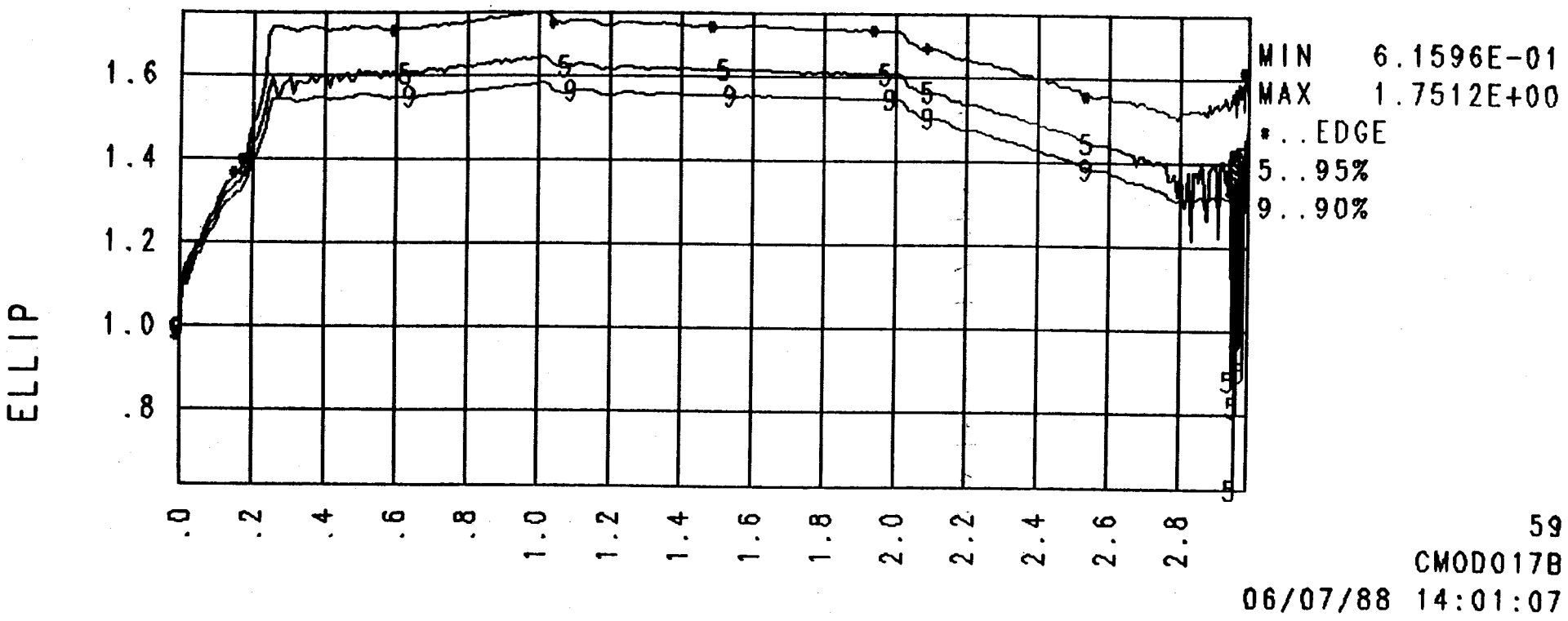
ELLIP
1.6
1.4
1.2
1.0
.8
.0
.2
.4
.6
.8
1.0
1.2
1.4
1.6
1.8
2.0
2.2
2.4
2.6
2.8
MIN 6.1596E-01
MAX 1.7512E+00
*..EDGE
5..95%
9..90%
59
CMOD017B
06/07/88 14:01:07

Fig. 10

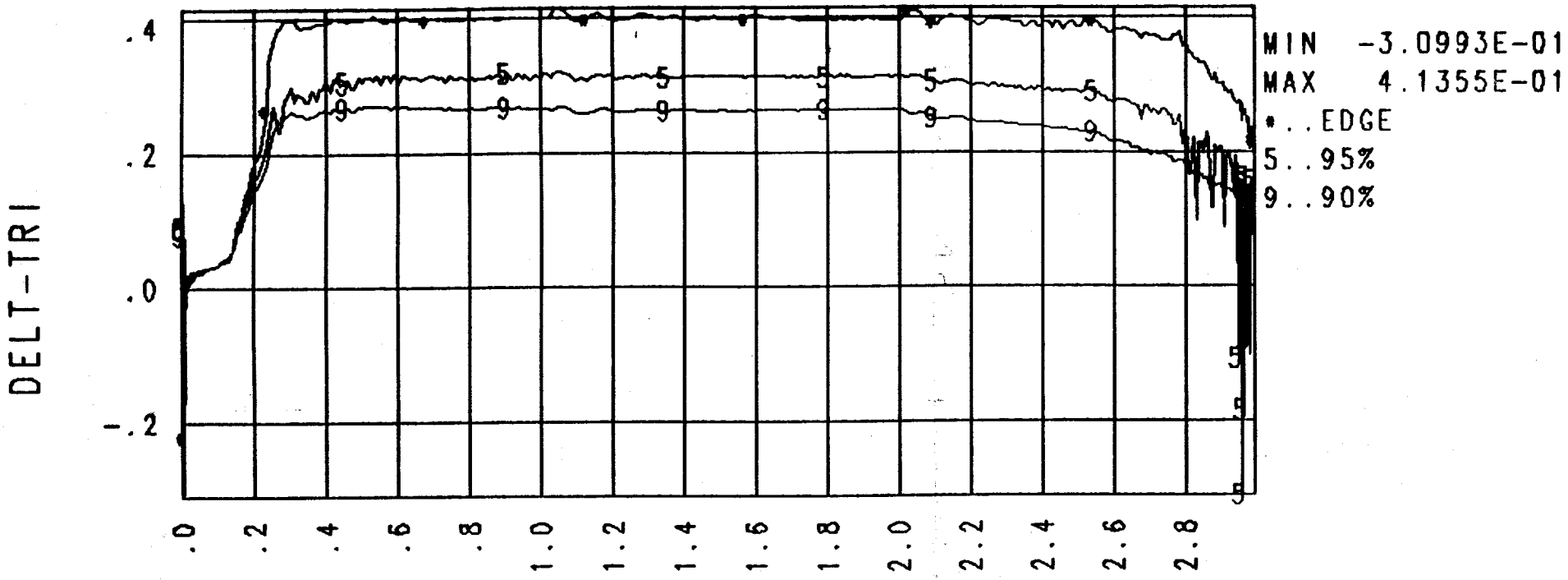
DELT-TRI
.4
.2
.0
-.2
.0
.2
.4
.6
.8
1.0
1.2
1.4
1.6
1.8
2.0
2.2
2.4
2.6
2.8
MIN -3.0993E-01
MAX 4.1355E-01
*..EDGE
5..95%
9..90%

Fig. 11

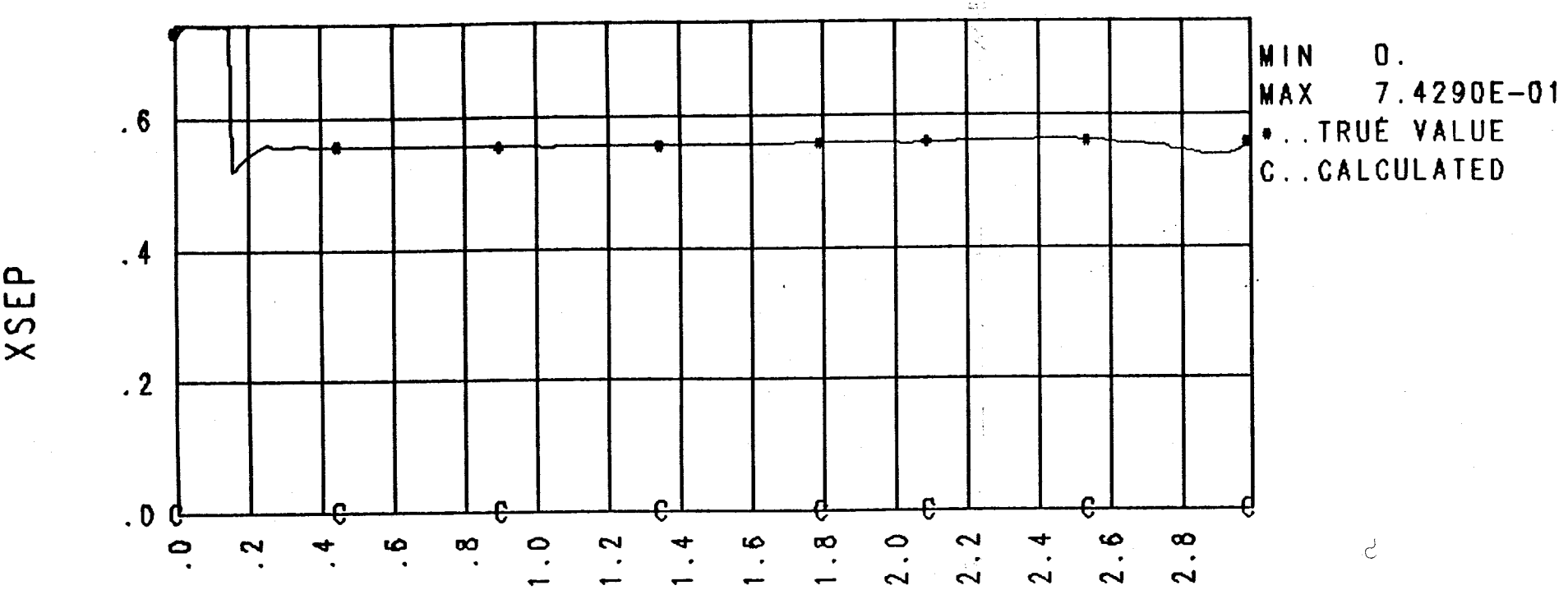
XSEP
.6
.4
.2
.0
.0
.2
.4
.6
.8
1.0
1.2
1.4
1.6
1.8
2.0
2.2
2.4
2.6
2.8
MIN 0.
MAX 7.4290E-01
*..TRUE VALUE
C..CALCULATED

Fig. 12

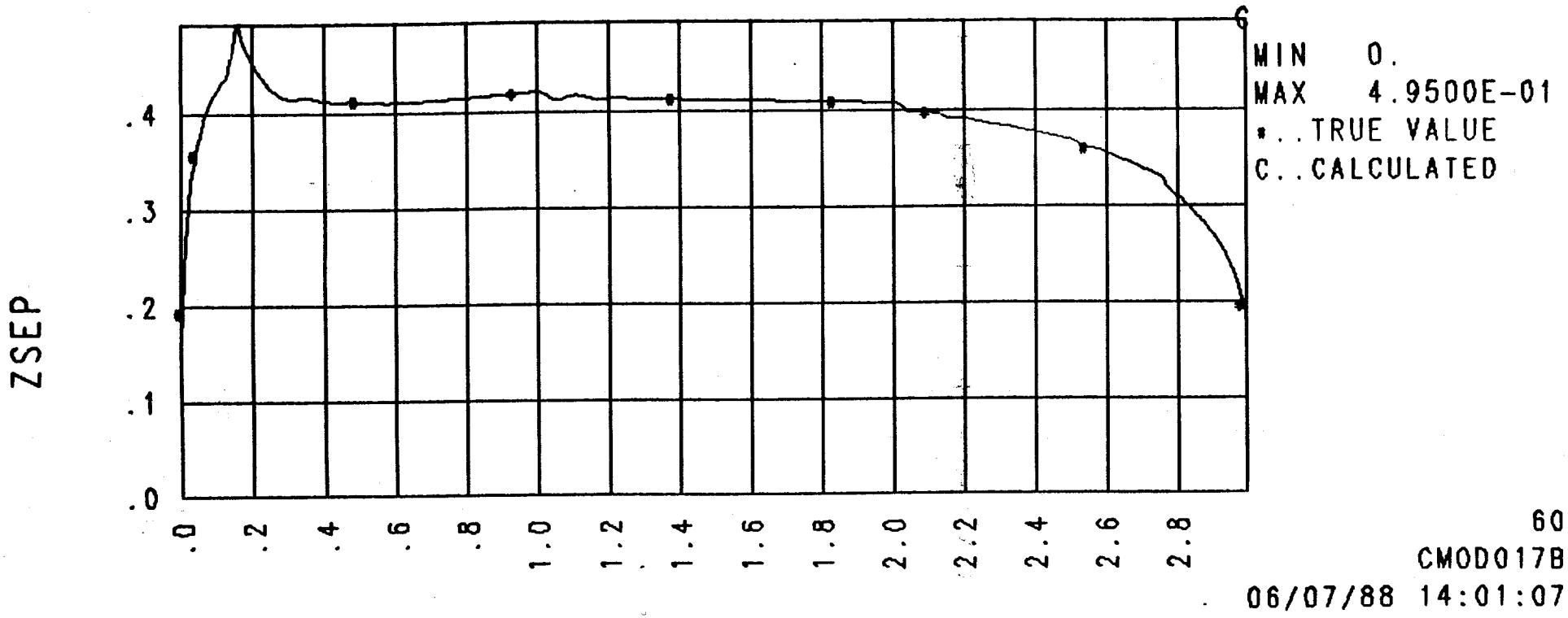
ZSEP
.4
.3
.2
.1
.0
.0
.2
.4
.6
.8
1.0
1.2
1.4
1.6
1.8
2.0
2.2
2.4
2.6
2.8
MIN 0.
MAX 4.9500E-01
*..TRUE VALUE
C..CALCULATED
60
CMOD017B
06/07/88 14:01:07

Fig. 13

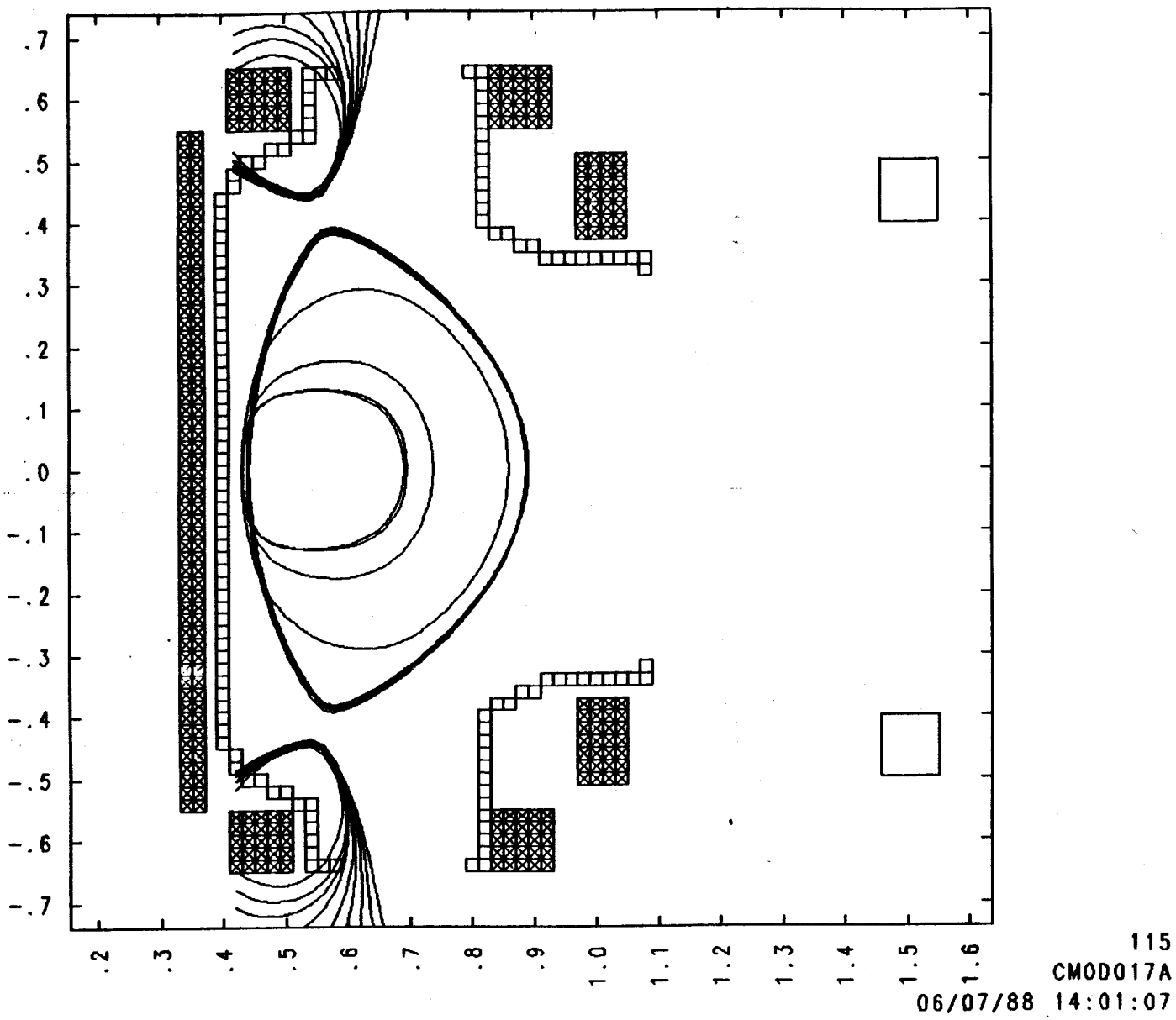
.7
.6
.5
.4
.3
.2
.1
.0
-.1
-.2
-.3
-.4
-.5
-.6
-.7
.2
.3
.4
.5
.6
.7
.8
.9
1.0
1.1
1.2
1.3
1.4
1.5
1.6
115
CMOD017A
06/07/88 14:01:07

Fig. 14

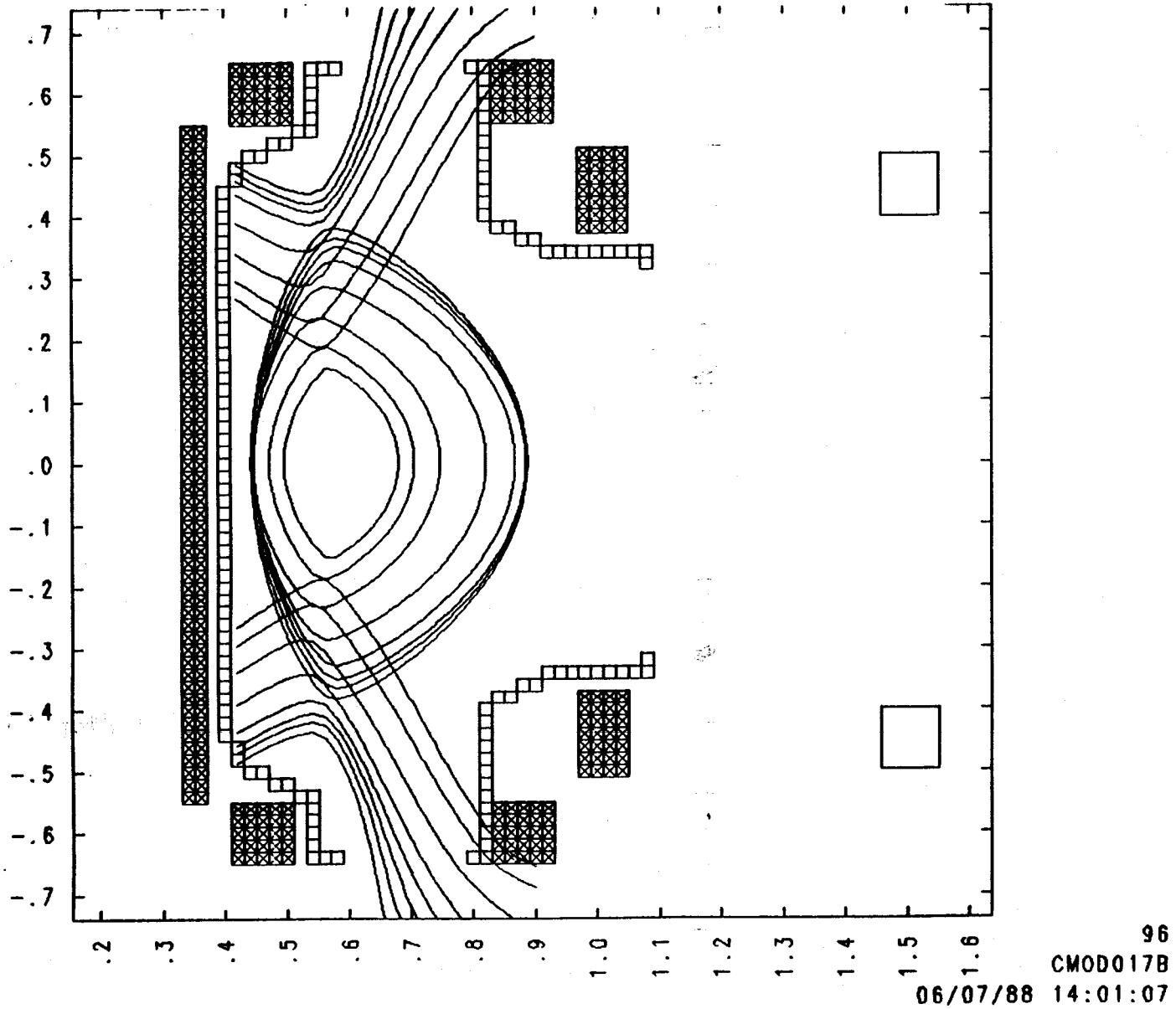
.7
.6
.5
.4
.3
.2
.1
.0
-.1
-.2
-.3
-.4
-.5
-.6
-.7
.2
.3
.4
.5
.6
.7
.8
.9
1.0
1.1
1.2
1.3
1.4
1.5
1.6
96
CMOD017B
06/07/88 14:01:07

Fig. 15

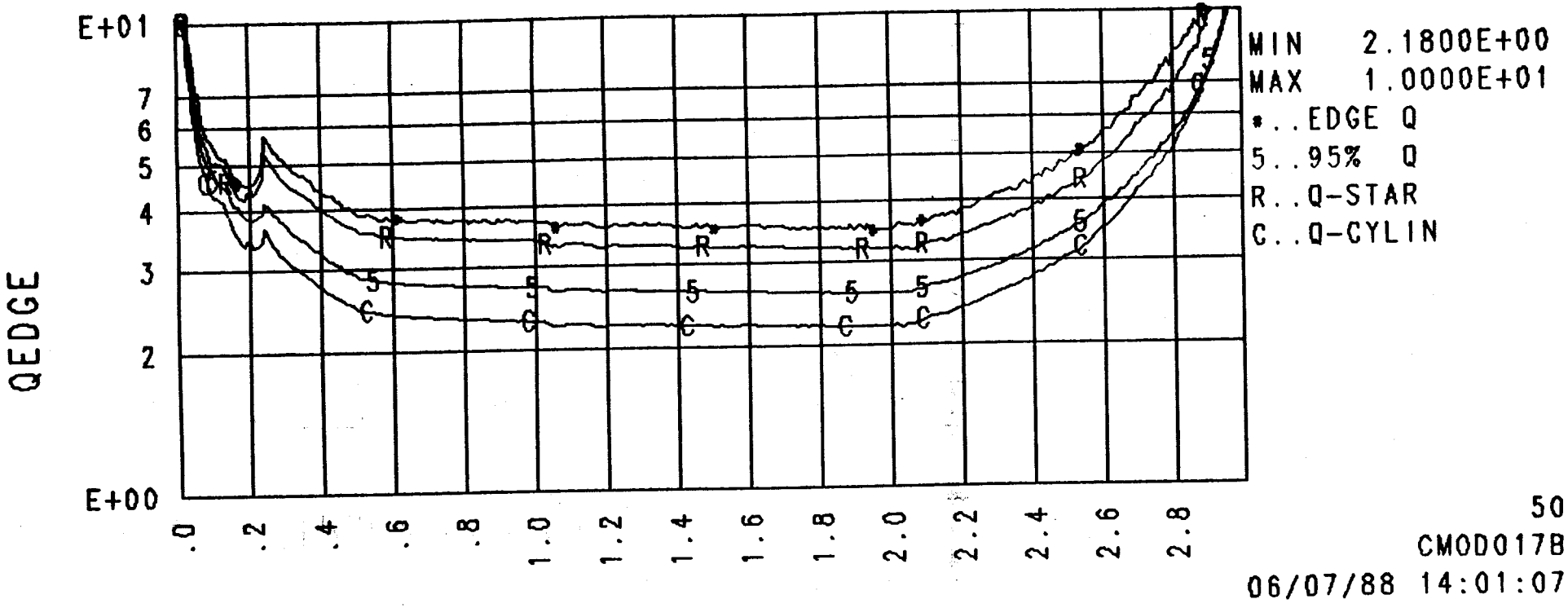
QEDGE
E+01
7
6
5
4
3
2
E+00
.0
.2
.4
.6
.8
1.0
1.2
1.4
1.6
1.8
2.0
2.2
2.4
2.6
2.8
MIN 2.1800E+00
MAX 1.0000E+01
*..EDGE Q
5..95% Q
R..Q-STAR
C..Q-CYLIN
50
CMOD017B
06/07/88 14:01:07

Fig. 16

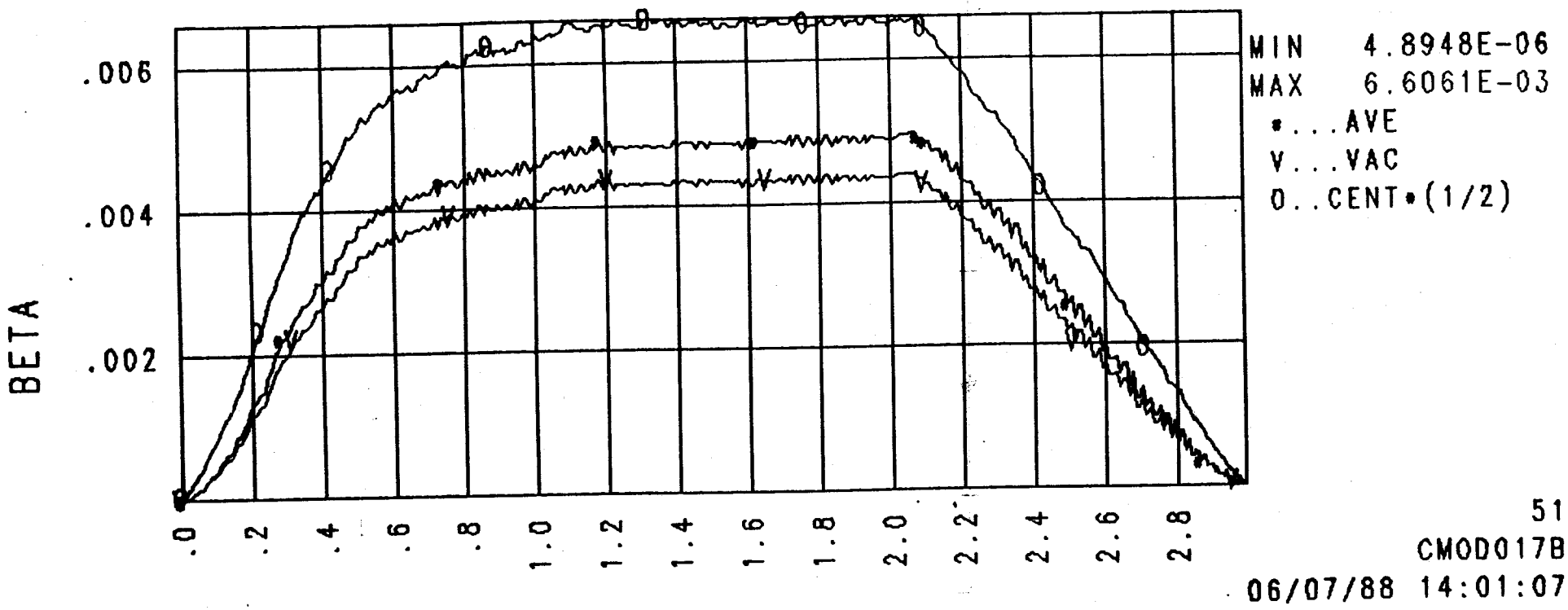
BETA
.006
.004
.002
.0
.2
.4
.6
.8
1.0
1.2
1.4
1.6
1.8
2.0
2.2
2.4
2.6
2.8
MIN 4.8948E-06
MAX 6.6061E-03
*...AVE
V...VAC
0..CENT*(1/2)
51
CMOD017B
06/07/88 14:01:07

Fig. 17

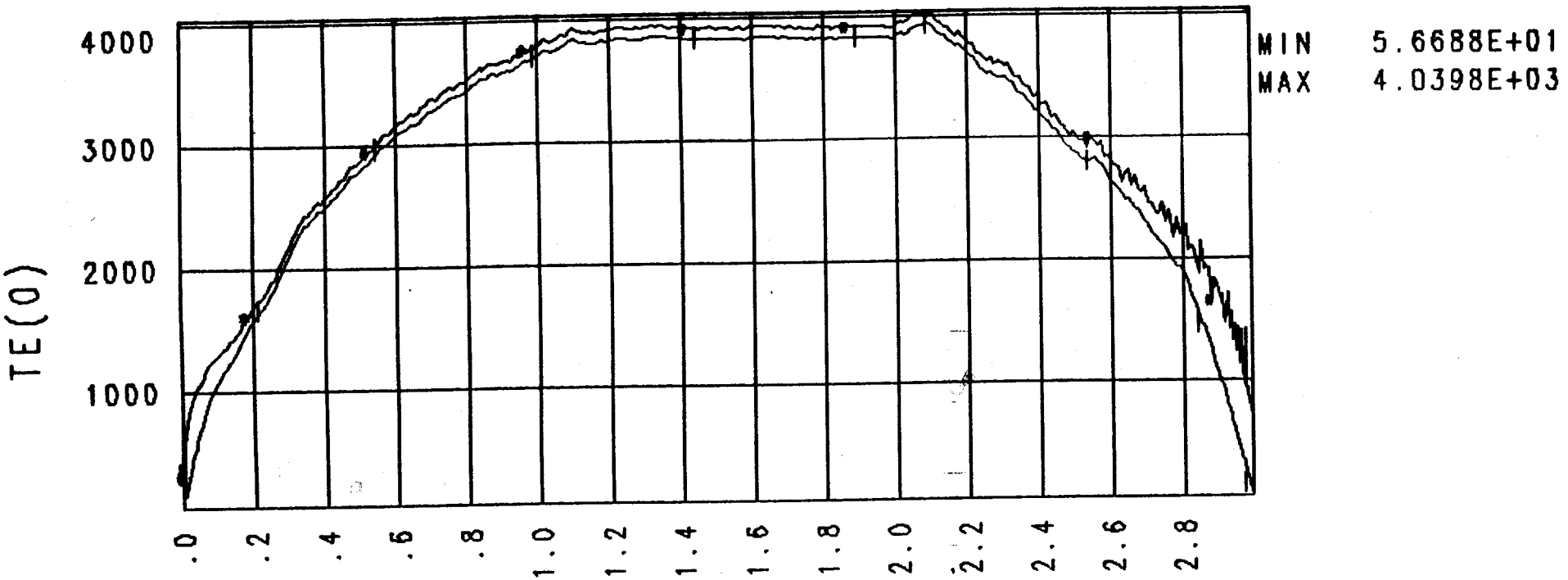
TE(0)
4000
3000
2000
1000
.0
.2
.4
.6
.8
1.0
1.2
1.4
1.6
1.8
2.0
2.2
2.4
2.6
2.8
MIN 5.6688E+01
MAX 4.0398E+03

Fig. 18

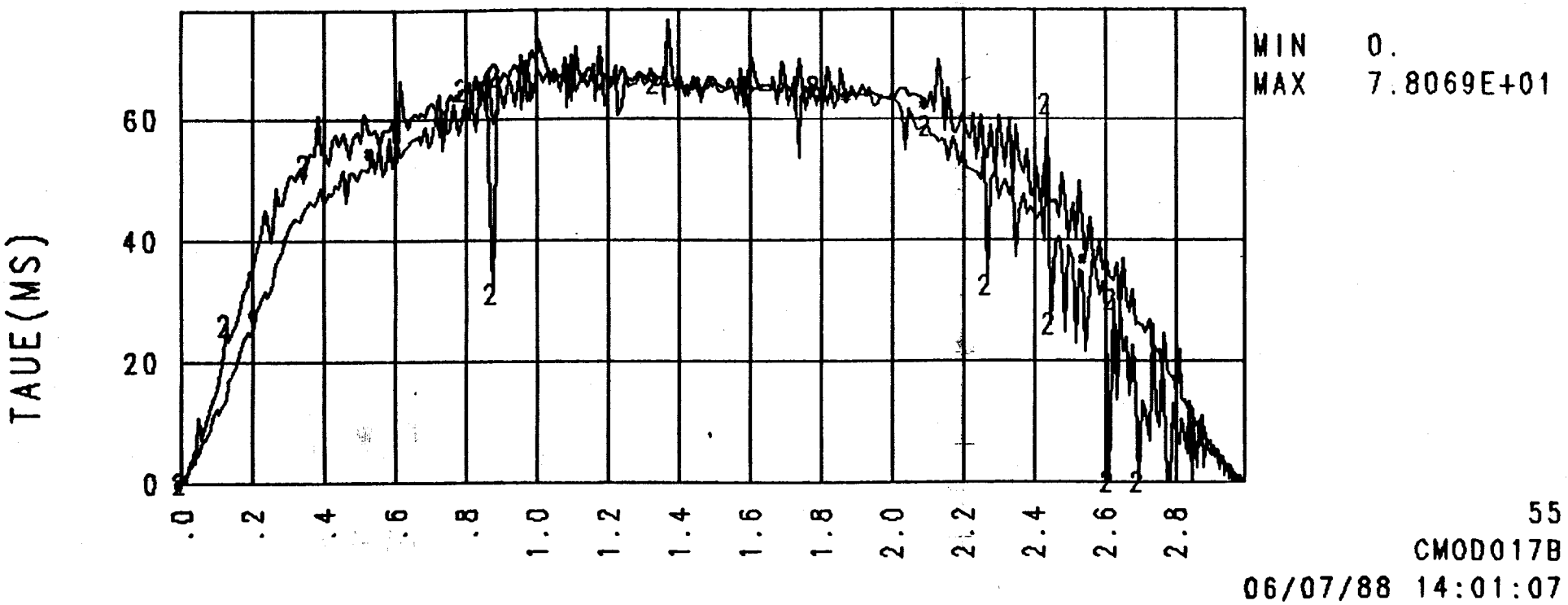
TAUE(MS)
0
20
40
60
.0
.2
.4
.6
.8
1.0
1.2
1.4
1.6
1.8
2.0
2.2
2.4
2.6
2.8
MIN 0.
MAX 7.8069E+01
55
CMOD017B
06/07/88 14:01:07

Fig. 19

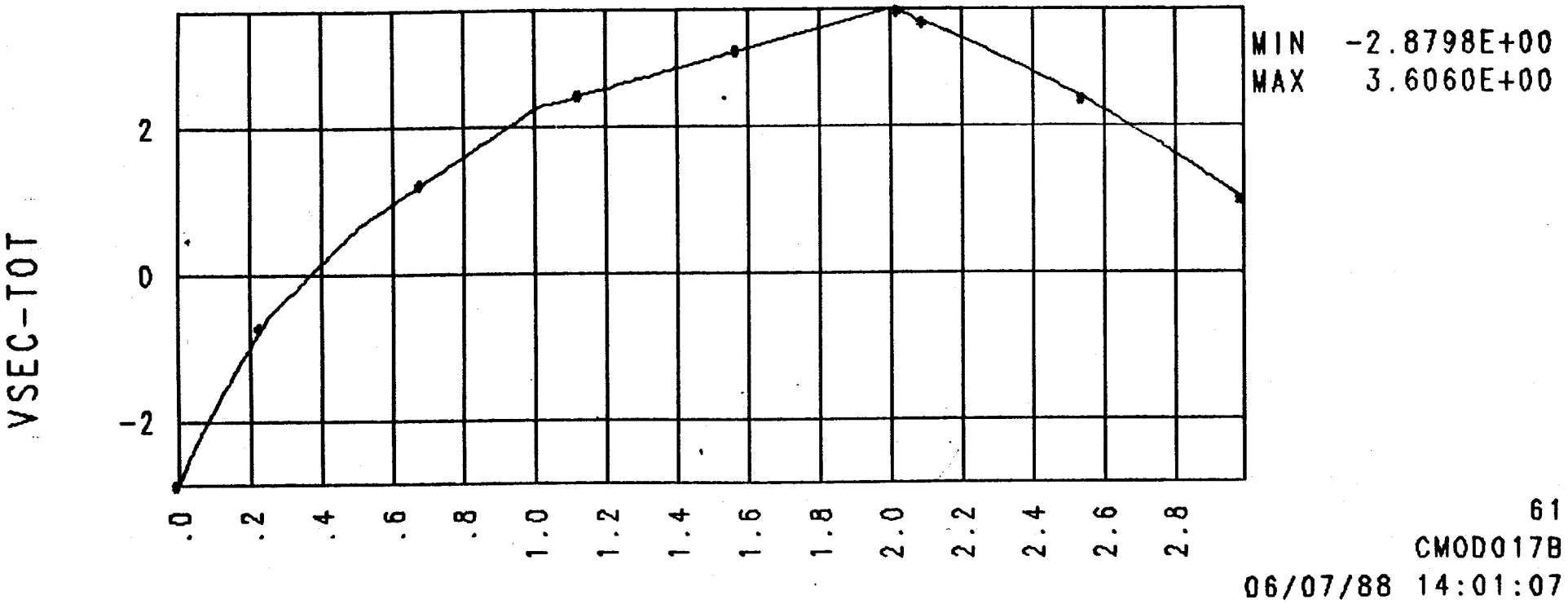
VSEC-TOT
2
0
-2
.0
.2
.4
.6
.8
1.0
1.2
1.4
1.6
1.8
2.0
2.2
2.4
2.6
2.8
MIN -2.8798E+00
MAX 3.6060E+00
61
CMOD017B
06/07/88 14:01:07

Fig. 20

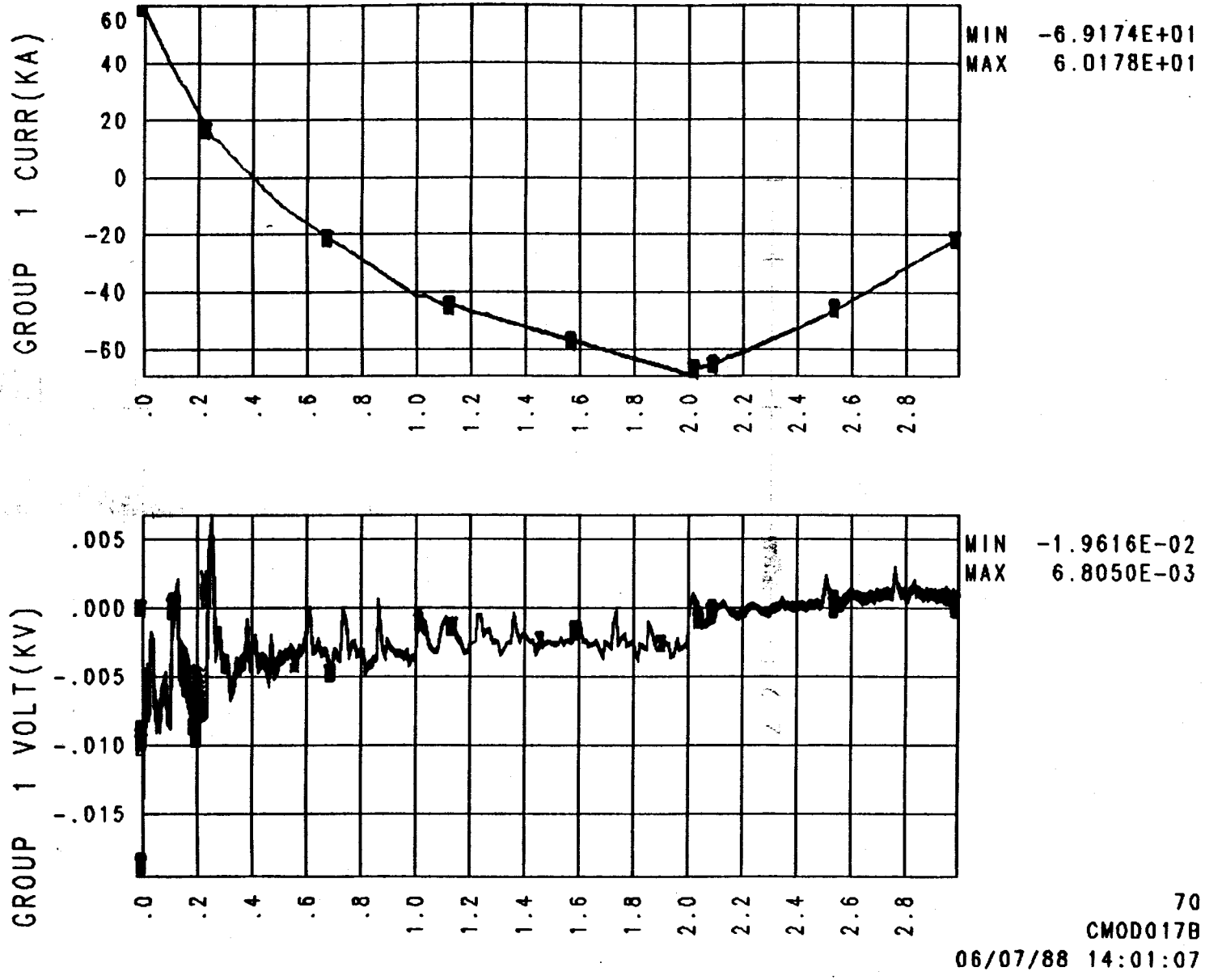
GROUP 1 CURR(KA)
60
40
20
0
-20
-40
-60
.0
.2
.4
.6
.8
1.0
1.2
1.4
1.6
1.8
2.0
2.2
2.4
2.6
2.8
MIN -6.9174E+01
MAX 6.0178E+01
GROUP 1 VOLT(KV)
.005
.000
-.005
-.010
-.015
MIN -1.9616E-02
MAX 6.8050E-03
70
CMOD017B
06/07/88 14:01:07

Fig. 21

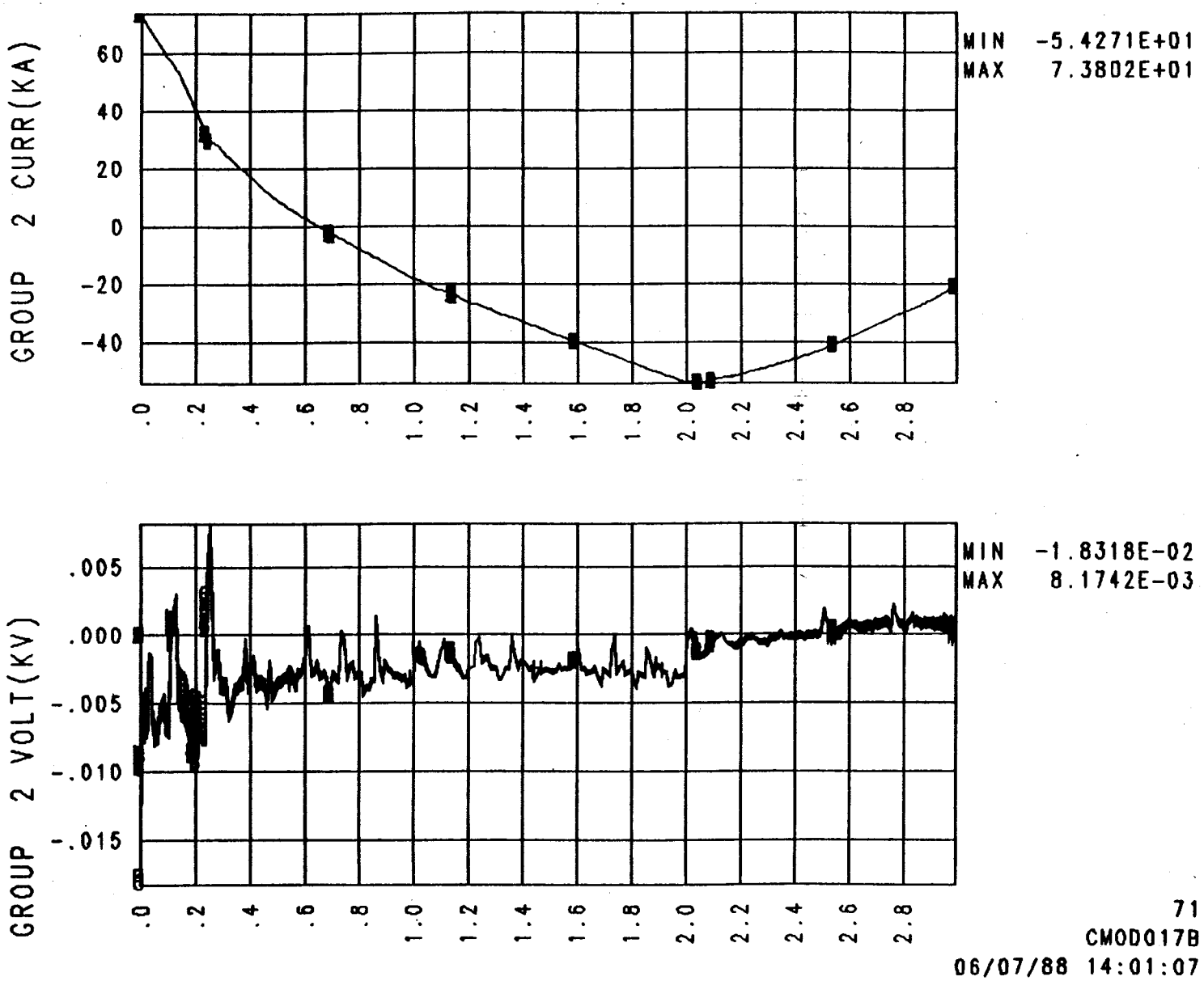
GROUP 2 CURR(KA)
60
40
20
0
-20
-40
.0
.2
.4
.6
.8
1.0
1.2
1.4
1.6
1.8
2.0
2.2
2.4
2.6
2.8
MIN -5.4271E+01
MAX 7.3802E+01
GROUP 2 VOLT(KV)
.005
.000
-.005
-.010
-.015
MIN -1.8318E-02
MAX 8.1742E-03
71
CMOD017B
06/07/88 14:01:07

Fig. 22

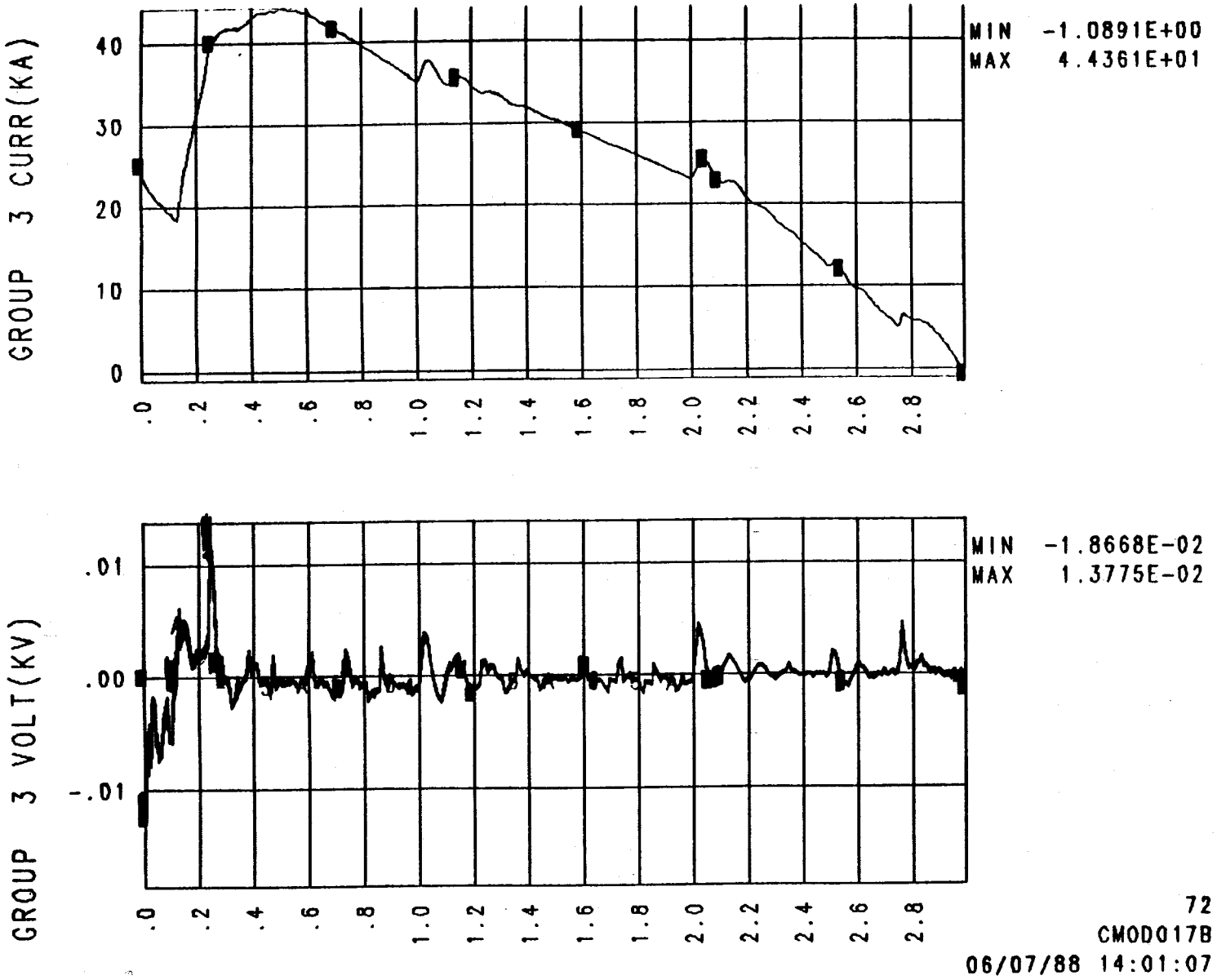
GROUP 3 CURR(KA)
40
30
20
10
0
.0
.2
.4
.6
.8
1.0
1.2
1.4
1.6
1.8
2.0
2.2
2.4
2.6
2.8
MIN -1.0891E+00
MAX 4.4361E+01
GROUP 3 VOLT(KV)
.01
.00
-.01
MIN -1.8668E-02
MAX 1.3775E-02
72
CMOD017B
06/07/88 14:01:07

Fig. 23

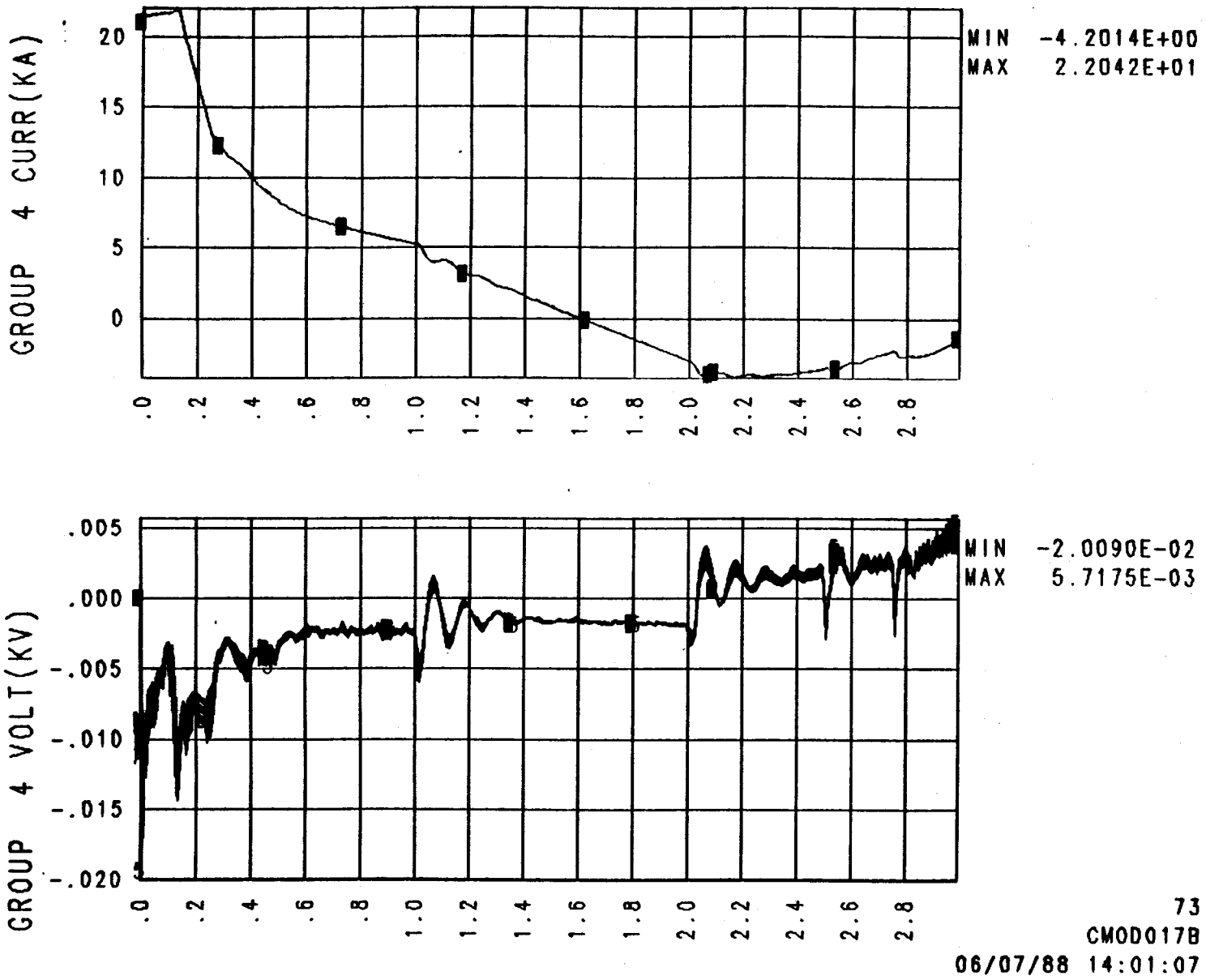
GROUP 4 CURR(KA)
20
15
10
5
0
.0
.2
.4
.6
.8
1.0
1.2
1.4
1.6
1.8
2.0
2.2
2.4
2.6
2.8
MIN -4.2014E+00
MAX 2.2042E+01
GROUP 4 VOLT(KV)
.005
.000
-.005
-.010
-.015
-.020
MIN -2.0090E-02
MAX 5.7175E-03
73
CMOD017B
06/07/88 14:01:07

Fig. 24

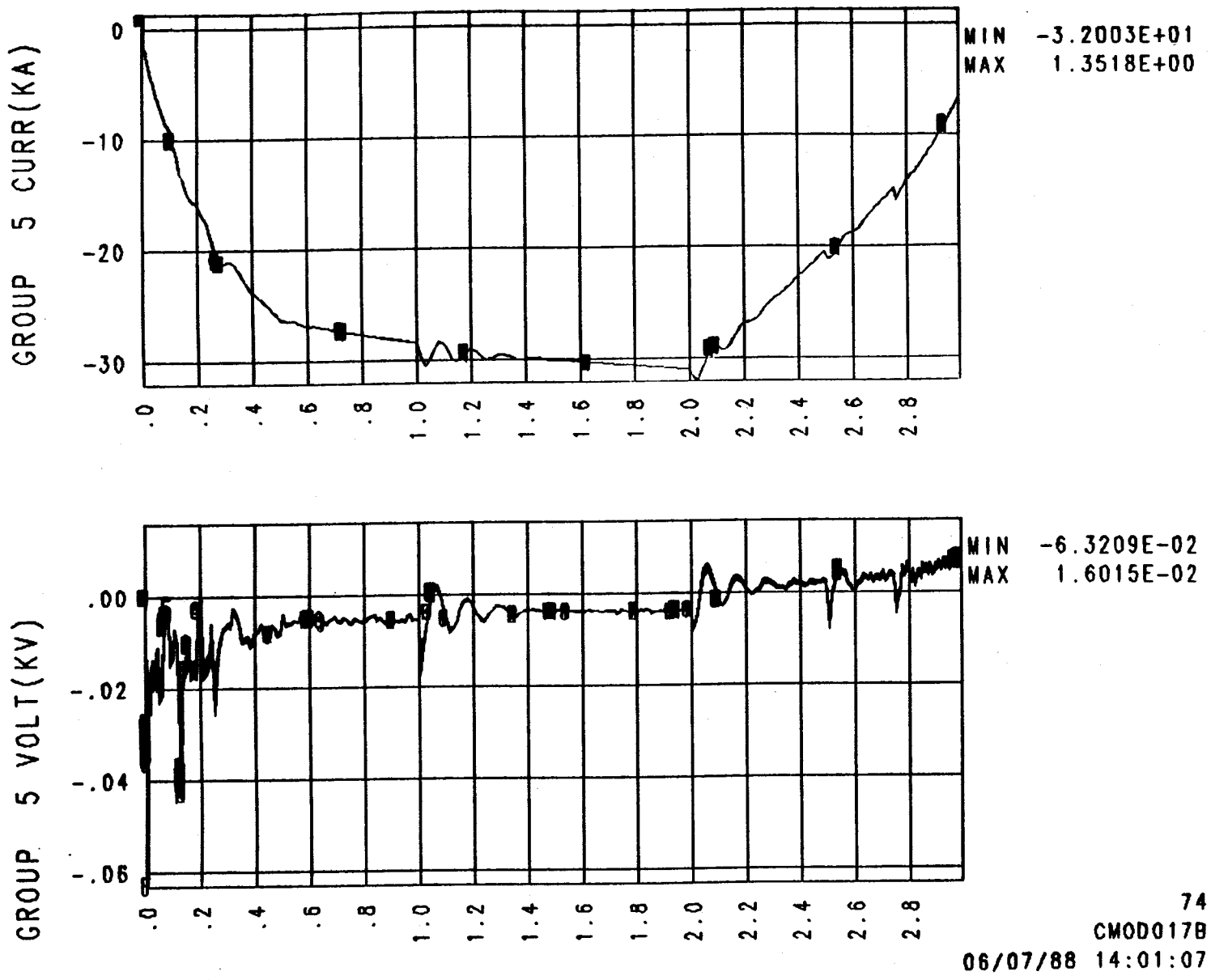
GROUP 5 CURR(KA)
0
-10
-20
-30
.0
.2
.4
.6
.8
1.0
1.2
1.4
1.6
1.8
2.0
2.2
2.4
2.6
2.8
MIN -3.2003E+01
MAX 1.3518E+00
GROUP 5 VOLT(KV)
.00
-.02
-.04
-.06
MIN -6.3209E-02
MAX 1.6015E-02
74
CMOD017B
06/07/88 14:01:07

Fig. 25

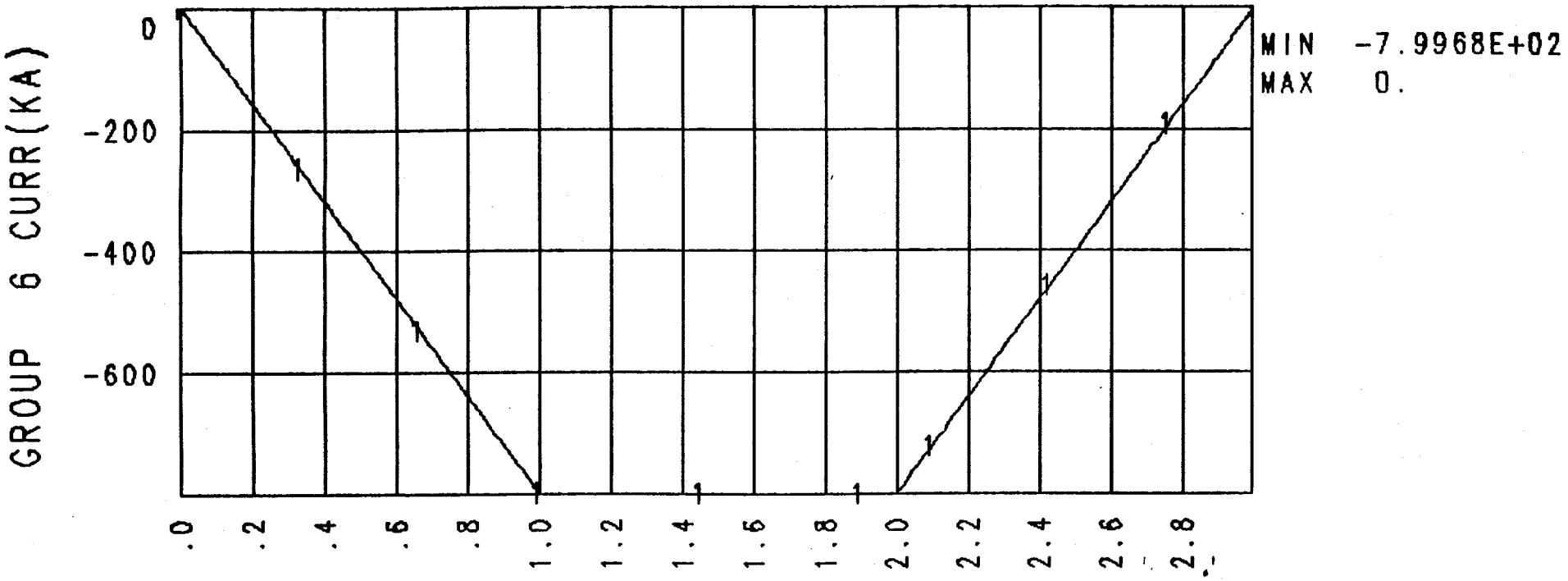
GROUP 6 CURR(KA)
0
-200
-400
-600
.0
.2
.4
.6
.8
1.0
1.2
1.4
1.6
1.8
2.0
2.2
2.4
2.6
2.8
MIN -7.9968E+02
MAX 0.

Fig. 26

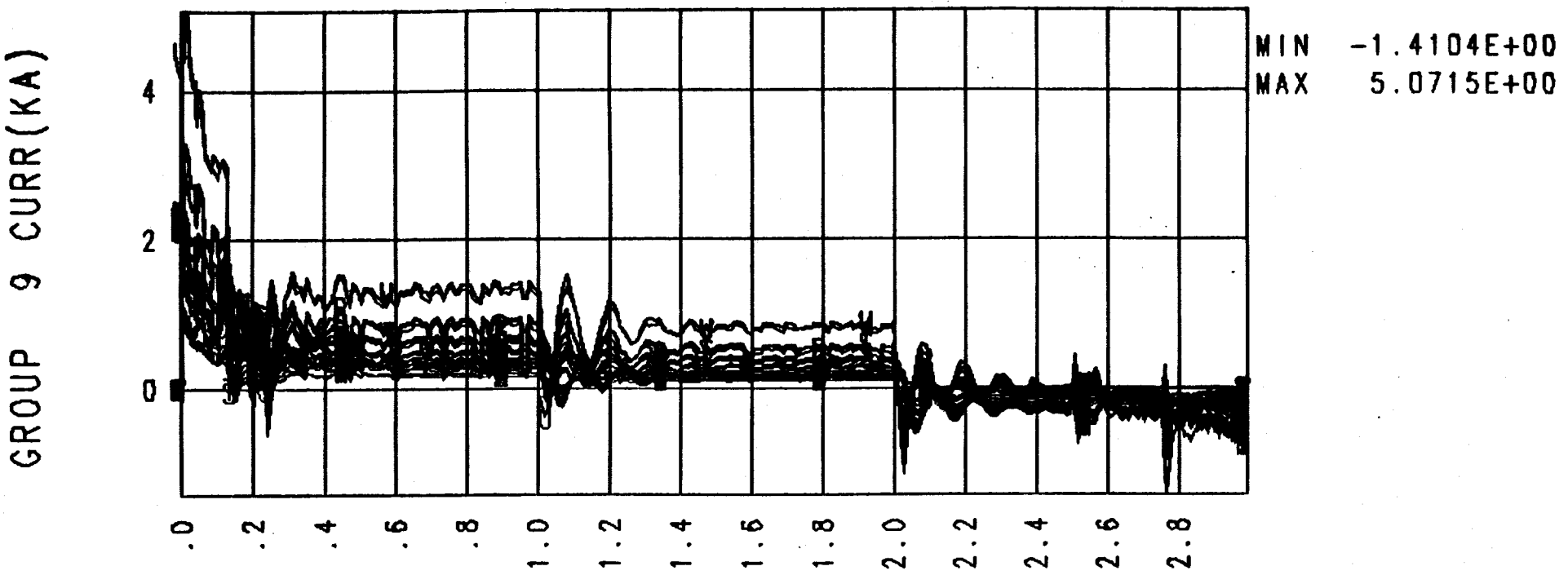
GROUP 9 CURR(KA)
4
2
0
.0
.2
.4
.6
.8
1.0
1.2
1.4
1.6
1.8
2.0
2.2
2.4
2.6
2.8
MIN -1.4104E+00
MAX 5.0715E+00

Fig. 27

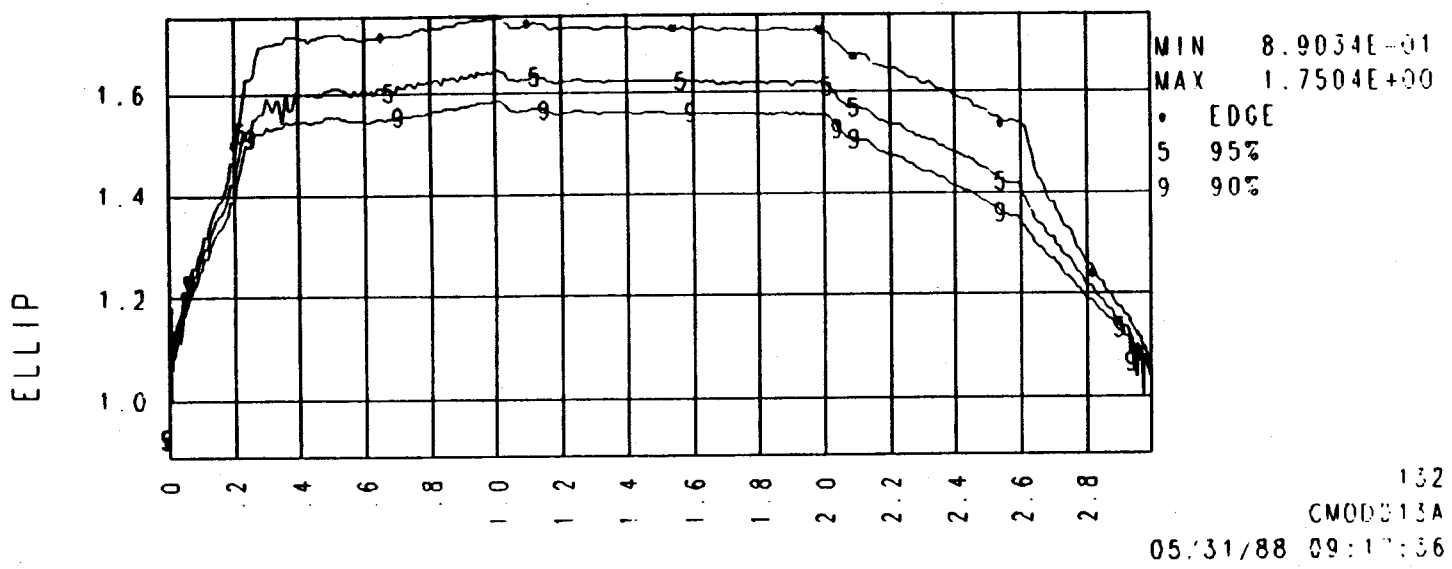
ELLIP
1.6
1.4
1.2
1.0
0
.2
.4
.6
.8
1.0
1.2
1.4
1.6
1.8
2.0
2.2
2.4
2.6
2.8
MIN 8.9034E-01
MAX 1.7504E+00
• EDGE
5 95%
9 90%
132
CMOD313A
05/31/88 09:17:56

Fig. 28

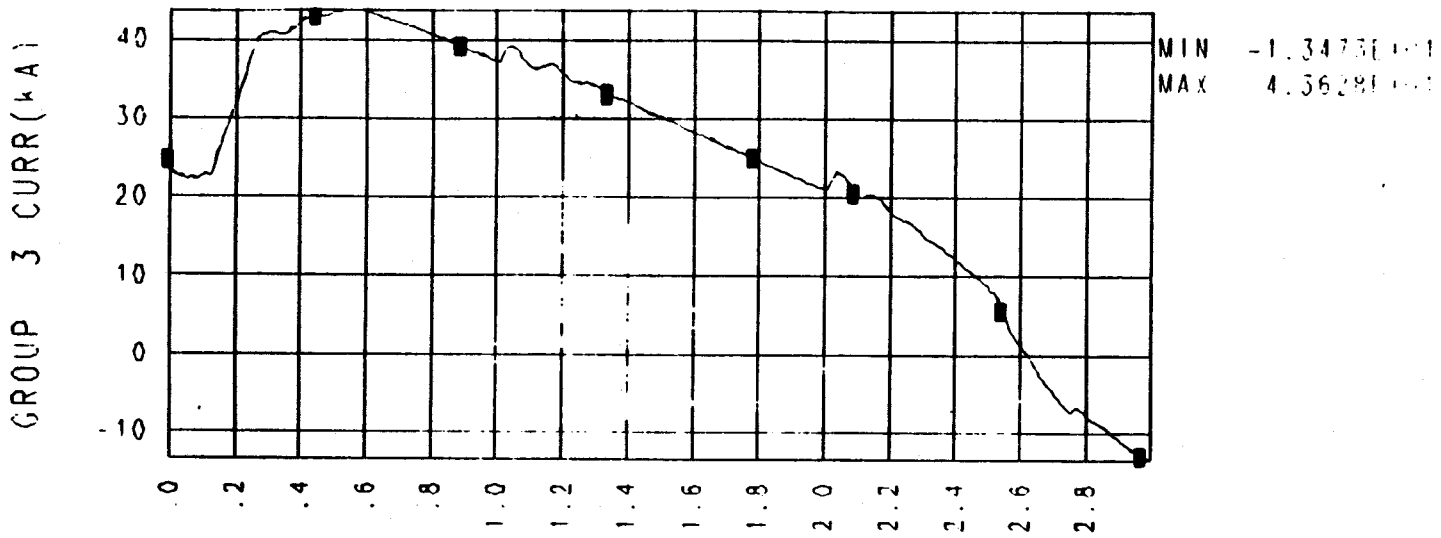
GROUP 3 CURR(kA)
40
30
20
10
0
-10
.0
.2
.4
.6
.8
1.0
1.2
1.4
1.6
1.8
2.0
2.2
2.4
2.6
2.8
MIN
MAX

Fig. 29